REPORT DOCUMENTATION PAGE

Public reporting burden for this collection of information is estimated to average 1 hour per response, including the time for reviewing instructions, searching existing data sources, gathering and maintaining the data needed, and completing and reviewing the collection of information. Send comments regarding this burden estimate or any other aspect of this collection of information, including suggestions for reducing this burden, to Washington Headquarters Services, Directorate for Information Operations and Reports, 1215 Jefferson Davis Highway, Suite 1204, Arlington, VA 22202-4302, and to the Office of Management and Budget, Paperwork Reduction Project (0704-0100), Washington, DC 20503.

1. AGENCY USE ONLY (Leave blank)	2. REPORT DATE	3. REPORT TYPE AND DATES COVERED
		FINAL REPORT - 01 Nov 93 - 31 Aug 96

4. TITLE AND SUBTITLE

~~INTEGRATION OF FERROELECTRIC THIN FILMS SLM'S AND OPTICAL INFORMATION PROCESSING SYSTEMS~~ *See Cover*

5. FUNDING NUMBERS

62712E
A569/03

6. AUTHOR(S)

Dr Neurgaonkar

7. PERFORMING ORGANIZATION NAME(S) AND ADDRESS(ES)

Rockwell Science Center
1049 Camino Dos Rios
Thousand Oaks, CA 91360

AFOSR-TR-96

013 97

9. SPONSORING / MONITORING AGENCY NAME(S) AND ADDRESS(ES)

AFOSR/NE
110 Duncan Avenue Suite B115
Bolling AFB DC 20332-8050

10. SPONSORING / MONITORING AGENCY REPORT NUMBER

0-94-C-0004

11. SUPPLEMENTARY NOTES

19970228 094

12a. DISTRIBUTION / AVAILABILITY STATEMENT

APPROVED FOR PUBLIC RELEASE: DISTRIBUTION UNLIMITED

12b. DISTRIBUTION CODE

13. ABSTRACT (Maximum 200 words)

High polarization PZT thin films have been grown on lattice-matched SBN and LAAlO3 substrates. The polarization obtained is the highest to-date, because these films are highly oriented. Because of incsreased polarization, the optical figure of merit is very high, which will produce compact devices operating at significantly lower voltages in applications such as guided-wave optics, switches and photorefractive memory.

[DTIC QUALITY INSPECTED 2

14. SUBJECT TERMS			15. NUMBER OF PAGES
			16. PRICE CODE

17. SECURITY CLASSIFICATION OF REPORT	18. SECURITY CLASSIFICATION OF THIS PAGE	19. SECURITY CLASSIFICATION OF ABSTRACT	20. LIMITATION OF ABSTRACT
UNCLASSIFIED	UNCLASSIFIED	UNCLASSIFIED	

SC71093FTR

Copy No. __3__

INTEGRATION OF FERROELECTRIC/SEMICONDUCTOR THIN FILMS FOR SLM AND PHOTOREFRACTIVE APPLICATIONS

FINAL TECHNICAL REPORT
For the Period
NOVEMBER , 1993 through August, 1996

CONTRACT NO. F49620-94-C-0004

Prepared for

Air Force Office of Scientific Research
Bolling AFB
Washington, DC 20332

R.R. Neurgaonkar
Principal Investigator

February, 1997

Approved for public release; distribution unlimited

DISCLAIMER NOTICE

REPORT DOCUMENTATION PAGE

FORM APPROVED
OMB No. 0704-0188

1a. REPORT SECURITY CLASSIFICATION	1b. RESTRICTIVE MARKINGS
UNCLASSIFIED	

2a. SECURITY CLASSIFICATION AUTHORITY	3. DISTRIBUTION/AVAILABILITY OF REPORT
2b. CLASSIFICATION/DOWNGRADING SCHEDULE	

4. PERFORMING ORGANIZATION REPORT NUMBER(S)	5. MONITORING ORGANIZATION REPORT NUMBER(S)
SC71093.FTR	

6a. NAME OF PERFORMING ORGANIZATION	6b. OFFICE SYMBOL *(If Applicable)*	7a. NAME OF MONITORING ORGANIZATION
Rockwell Science Center, Inc.		

6c. ADDRESS *(City, State and ZIP Code)*	7b. ADDRESS *(City, State and ZIP Code)*
P.O. Box 1085 **Thousand Oaks , CA 91358**	

8a. NAME OF FUNDING/SPONSORING ORGANIZATION	8b. OFFICE SYMBOL *(If Applicable)*	9. PROCUREMENT INSTRUMENT IDENTIFICATION NUMBER
		Contract No. 49620-94-C-0004

8C. ADDRESS *(City, State and ZIP Code)*	10. SOURCE OF FUNDING NOS.			
	PROGRAM ELEMENT NO.	PROJECT NO.	TASK NO.	WORK UNIT ACCESSION NO.

11. TITLE *(Include Security Classification)*

Integration of Ferroelectric/Semiconductor Thin Films for SLM and Photorefractive Applications

12. PERSONAL AUTHOR(S)

Neurgaonkar, Ratnakar, R.

13a. TYPE OF REPORT	13b. TIME COVERED	14. DATE OF REPORT *(Year, Month, Day)*	15. PAGE COUNT
Final Report	FROM *Nov 1993* TO *Aug 1996*	**1997, February 14**	**35**

16. SUPPLEMENTARY NOTATION

Reproduction in whole or in part is permitted for any purpose of the United States Government.

17.	COSATI CODES		18. SUBJECT TERMS *(Continue on reverse if necessary and identify by block number)*
FIELD	GROUP	SUB-GROUP	*Electro-optic, photorefractive, guided-wave, thin films, sol-gel,*
			lattice-match, SBN, LaAlO$_3$

19. ABSTRACT *(Continue on reverse if necessary and identify by block number)*

High polarization PZT thin films have been grown on lattice-matched SBN and LaAlO$_3$ substrates. The polarization obtained is the highest to-date (35°C/cm^2), because these films are highly oriented. Because of increased polarization, the optical figure of merit is very high, which will produce compact devices operating at significantly lower voltages in applications such as guided-wave optics, switches and photorefractive memory.

20. DISTRIBUTION/AVAILABILITY OF ABSTRACT	21. ABSTRACT SECURITY CLASSIFICATION
UNCLASSIFIED/UNLIMITED ☐ SAME AS RPT. ☒ DTIC USERS ☐	**UNCLASSIFIED**

22a. NAME OF RESPONSIBLE INDIVIDUAL	22b. TELEPHONE NUMBER *(INCLUDE AREA CODE)*	22c. OFFICE SYMBOL
R.R. Neurgaonkar	*(805) 373-4109*	

DD FORM 1473   Previous editions are obsolete.   **UNCLASSIFIED**

TABLE OF CONTENTS

LIST OF FIGURES

LIST OF TABLES

1.0   ABSTRACT

This report covers work on the integration of ferroelectric and semiconductor materials for spatial light modulators (SLMs) carried from November, 1993 through August, 1996 in the Ferroelectric and Optical Materials Department of the Rockwell International Science Center under Contract No. F49620-94-C-0084. During this period, significant progress was made in the growth of highly grain-oriented perovskite PZT and $BaTiO_3$ thin films on lattice matched $LaAlO_3$ and SBN substrates for photorefractive applications. The oriented PZT films show high polarization in the range of 30-35 $\mu C/cm^2$, indicating the strong electro-optic effect necessary for photorefractive applications. This report also includes the growth of individual PZT and SBN:75 thin films on SBN:60 and semiconducting Si substrates, and the successful fabrication of ferroelectric multilayers consisting of alternating PZT and SBN films for spatial light modulators (SLMs). Measurements of optical modulation were carried out on multilayer stack thin film which confirmed the increase in modulation depth with number of layers. This is significant advances towards fabrication a practical modulators.

The films grown under this program will have impact on the following applications:

1. SLM's	Stack PZT/SBN films	Interconnects.
2. Photorefractive	$BaTiO_3$ and SBN on SBN	Pattern recognition, 3-D memory.
3. Guided-Wave	PZT on SBN	Telecommunication, Switches.
4. Electronic memory	PZT on Si	F-Ram and D-Ram.

Besides photorefractive and SLM applications, the new high polarization PZT films grown on SBN are potentially useful for achieving low operating voltages in guided-wave structures (Such structures are being designed for telecommunication and signal processing systems), while films grown on Si are potentially useful for electronic memory applications.

2.0 INTRODUCTION

The objective of the this program was to produce high quality, high refractive index ferroelectric thin films for applications in spatial light modulators (SLM's) and photorefractive applications. These devices may include image processing, photorefractive channel waveguides, optical signal filters, optical neural computing and other types of devices. The development of ferroelectric thin films for SLM and photorefractive applications is summarized in Figure 2.1.

Ferroelectric Thin Films

PZT, BaTiO$_3$ PBN

Photorefractive Films
- $n^3 r_{ij}/\varepsilon$
- Response ~ 1 ms
- Coupling > 20 cm^{-1}

Electro-Optic Films
- r_{ij}/ε
- High Modulation
- Low Optical Loss

PZT, SBN

Substrate SBN | Dopants - Fe - Ce

Substrates SBN or Si | Undoped

- Polarization > 40 µc/cm^2
- Response: < 35 ms
- Single crystal films

- Polarization > 20 µc/cm^2
- High modulation
- Grain-oriented films

Applications

- Pattern recognition
- Signal Processing
- 3-D memory & Storage

- Telecommunication
- Switches & Filters
- Signal Processing

Figure 2.1 - The development of ferroelectric thin films for SLM and photorefractive applications.

Using techniques that have become well-established at Rockwell, the fabrication of ferroelectric thin films grown on various substrates has been carefully studied with respect to film growth conditions, annealing temperature, substrate type and substrate orientation. After the samples were thoroughly characterized by our group, structures fabricated under this program are now being evaluated at the University of California, San Diego (Professor Sing Lee and Dr. Volkan Ozgus) and at the Rockwell International Science Center (Dr. John Hong) for possible use in the specific devices mentioned above.

3.0   PROGRESS SUMMARY AND MAJOR ACCOMPLISHMENTS

Table 3.1 summarizes the ferroelectric thin film materials selected for study under this program. The optical figures-of-merit for these materials are exceptionally good and currently we have established the sputtering and sol-gel growth techniques for PZT and SBN compositions. In our earlier experiments, we used tungsten bronze PBN:60 for the development of multilayer film stacks; however, our work shows that PZT and PBN react at elevated temperatures and only the tungsten bronze phase is crystallized. For this reason, we have selected PZT and SBN:75 for the multilayer stack work, where they have been grown individually and as alternating layers.

Table 3.1
Comparison of PZT, SBN and BaTiO$_3$ Material

Film Composition	n	rij	ε (x 10^{-12} m/V)	Tc (°C)	Substrates
PZT	2.456	> 2200	~2500	> 340	SBN or Si
PLZT	2.405	> 2500	>3000	~ 150	SBN or Si
PBN:60	2.401	> 2000	~1900	> 300	SBN or Si
BaTiO3	2.400	~ 600	~4600	> 120	SBN

n = refractive index, rij = electro-optic coeff., ε = dielectric constant

Table 3.2 summarizes the development of ferroelectric thin film structures for spatial light modulators (SLMs) and optical information processing systems (photorefractive effects) that has been proceeding at Rockwell International over the past 12 months. Substantial progress was made in establishing the best compositions and deposition conditions for electro-optic and photorefractive films using various substrates appropriate for each application.

For SLMs, the most significant accomplishment was the deposition of alternating PZT and SBN:75 layers on Pt-coated Si and SBN substrates. In the case of photorefractive films, we are the first group to deposit nearly single crystal PZT and BaTiO$_3$ thin films on lattice-matched SBN:60. These films contain dopants suitable for controlling photorefractive speed, coupling and diffraction efficiency. This work forms a basis for the development of specific device concepts. At UCSD, Professor Sing Lee and Volkan Ozgus have formulated several structural designs for SLMs based on our electro-optic multilayer thin film structures. At the Rockwell International Science Center, John Hong is also generating designs for various optical information processing functions using these photorefractive films.

3

Table 3.2
Growth Conditions for PZT Films

Substrate	Annealing Temp (°C)	Thickness (µm)	Film Orientation	Unit Cell (Å)
SBN Substrate				
(001) No Coating	640-675	0.5 to 1.5	(100) oriented	4.015
(001) LSC-Coating	620-640	0.5 to 1.0	(100) oriented	4.021
(100) No Coating	640-675	0.5 to 1.0	polycrystalline	-----
SrTiO3 Substrate				
(100) No Coating	620-635	0.5 to 1.0	(100) oriented	3.992
(100) LSC Coating	620-635	0.5 to 1.2	(100) oriented	3.995
MgO Substrate				
(100) No Coating	640-650	0.5 to 1.0	partially oriented	4.081
(100) LSC Coating	640-650	0.5 to 1.0	(100) oriented	4.081

3.1 Electro-Optic Thin Film Structures for SLM Applications

Thin electro-optic films are promising for applications where optical output has to be combined with electronic processing due to the process compatibility of thin film deposition with electronic manufacturing techniques. However, thin films have small modulation depths and require higher voltages to obtain the performance required by optoelectronic system applications. The use of multilayer structures can significantly reduce the required magnitude of the applied voltage for the operation of electro-optic devices.

Recent developments in technologies to obtain thin solid films of ferroelectric crystals have opened the possibility to fabricate electro-optic devices for highly parallel computer systems with superior properties compared to those devices that utilize bulk ferroelectric crystals, ferroelectric liquid crystals (FLC) or multiple quantum wells (MQW). FLC devices require the least amount of field strength for operation, but slow response times limit their application since the switching speeds of devices based on FLC cannot exceed a few kHz. On the other hand, MQW devices can operate at exceptional speeds (roughly in the GHz range), but they are inherently absorptive as their electro-optic behavior is based on field-controlled modification of the absorption peak;

4

absorption causes heat dissipation problems, limits optical throughput and, consequently, the number of fan-outs for parallel computing architectures. Bulk ferroelectric crystals such as 9/65/35 lead lanthanum zirconate titanate (PLZT), strontium barium niobate (SBN), or lead zirconate titanate (PZT) are transparent to visible and near-IR light and can be operated in the hundreds of MHz range. The transverse-mode spatial light modulator configuration in which they are typically employed do not take full advantage of their large linear or quadratic electro-optic coefficients, and consequently, the resulting devices typically have apertures less than 20 μm across to keep the operation voltages to less than 50 V. With the emergence of technologies to obtain ferroelectric multilayer films of these materials, all the benefits of utilizing multilayer designs can be realized to fabricate devices that are superior to multilayer-based FLC and MQW electro-optic devices.

The goal of this effort is to design, fabricate and characterize ferroelectric multilayers for optoelectronic device applications. UCSD is responsible for design and optimization of the multilayers in terms of thickness and material combinations, and Rockwell is responsible for fabricating the multilayer stacks with UCSD characterizing the fabricated structure.

3.2 Ferroelectric Multilayer Performance Optimization

Two application can be identified where multilayer thin films are beneficial: spatial light modulators and tunable filters.

Spatial Light Modulators (SLMs) are the basic building blocks in optical computing, information processing, display and optical interconnection systems. These devices modify the phase, polarization, amplitude and/or intensity of the light distribution under the control of an electrical input signal (electrically-addressed SLM) or another optical signal (optically-addressed SLM). When more functionality is needed, electronic processing can be added at each pixel element resulting in a structure referred to as a smart SLM (S-SLM) or smart pixels. Electrically or optically addressed, gray-scale capable, smart SLM's are key components for image processing, optoelectronic interconnection networks, neural networks and 3-D display applications [1-4].

A typical SLM using a bulk PLZT offers fast modulation (above 400 MHz), high contrast ratio (1000:1), low insertion losses (less than 10%) and high modulation depth (above 90%) at a half-wave voltage of about 200 V for a wide range of wavelengths. However, calculations indicate that a high reflector (HR) stack or a Fabry-Perot (FP) filter consisting of ferroelectric layers can be used to obtain similar performance at much lower voltage swings.

Standard designs for multilayer HR and FP filter stacks are depicted in Figure 3.1. Both types of devices consist of alternating layers of a high index and a low index films with quarter-wave optical thicknesses as defined by

$$t_i = \frac{\lambda}{4n_i},$$

Eq. (1)

where t_i is the i-th layer film thickness for layer with refractive index n_i. FP filters consist of symmetric HR stacks centered about a spacer layer that is an integral multiple of the half-wave optical thickness as shown in Figure 3.1. The spectral reflection curves for typical HR and FP filters are shown in Figures 3.2 and 3.3, respectively. As the characteristics of these stacks are determined by the principles of coherent interference, they are highly wavelength dependent. Any systematic deviation in the optical thickness of the layers can shift the entire spectrum in the wavelength space. With ferroelectric multilayer stacks, such deviation can be induced and varied intentionally by externally applying an electric field. When an electric field is applied to a ferroelectric film, the effective refractive index of the film changes while the physical dimension of the film remains almost unchanged. The change in refractive index approximately follows the equations,

$$n(V) = n_o - \tfrac{1}{2} n_o^3 \gamma_i \frac{V}{D}$$ (for linear material) Eq. (2)

$$n(V) = n_o - \tfrac{1}{2} n_o^3 \gamma_i \left(\tfrac{V}{D}\right)^2$$ (for quadratic material) Eq. (3)

where n_o is the refractive index in the absence of an external field, r_i is the electro-optic coefficient, D is the electrode spacing, and V is the voltage applied across the electrodes. Following Eqs. (2) and (3), the effective refractive indices each layer in the film reduces as a voltage is applied. Consequently, the spectral response curve of the multilayer stack should shift toward shorter wavelengths as the voltage is increased. If the stack is initially fabricated so that the operation wavelength falls on the reflection minimum closest to the stop band in the absence of a field, then application of a field should shift the stop band over the operation wavelength as indicated by the dotted curve in Figure 3.2. Thus, the transmission of the filter is changed from initial value of ~100% down to ~0% for only a few nanometer shift in the spectrum. A FP filter has a narrow transmission spike at the center of the stop band as shown in Figure 3.3. If all the layers in the stack are ferroelectric, its operation follows the same principles as the HR stack.

Surface Electrodes

ITO Electrodes

nL=2.337

SBN Substrate n~2.45

(a)

nL=2.337

SBN Substrate n~2.45

(b)

nL=2.337

Spacer n =2.618

Period = N1

Single (n+1) λ/2 layer

Period = N2

nL=2.337

SBN Substrate n~2.45

(c)

Figure 3.1 - Schematic illustration of a ferroelectric multilayer film device. (a) A transverse mode high reflector (HR) stack with surface electrodes. (b) A longitudinal mode HR stack with transparent ITO electrodes. (c) A symmetric fabry-perot filter. Aspect ratio has been exaggerated for illustration. A typical film stack thickness is ~2 μm, whereas the electrode spacing is ≥ 10 μm.

10(HL)-H Response

20(HL)-H Response

Figure 3.2 - Reflectance spectra of ferroelectric high reflector stacks: (a) 10 period stack and (b) 20 pair stack with 10 μm spaced surface electrodes at 0 V (solid) and 40 V (dashed).

11/94-FP2V= 40

Figure 3.3 - Reflectance spectra of ferroelectric Fabry-Perot filter with 10 μm spaced surface electrodes at 0 V (solid) and 40 V (dashed). Note the narrow (~1nm) pass-band in the center.

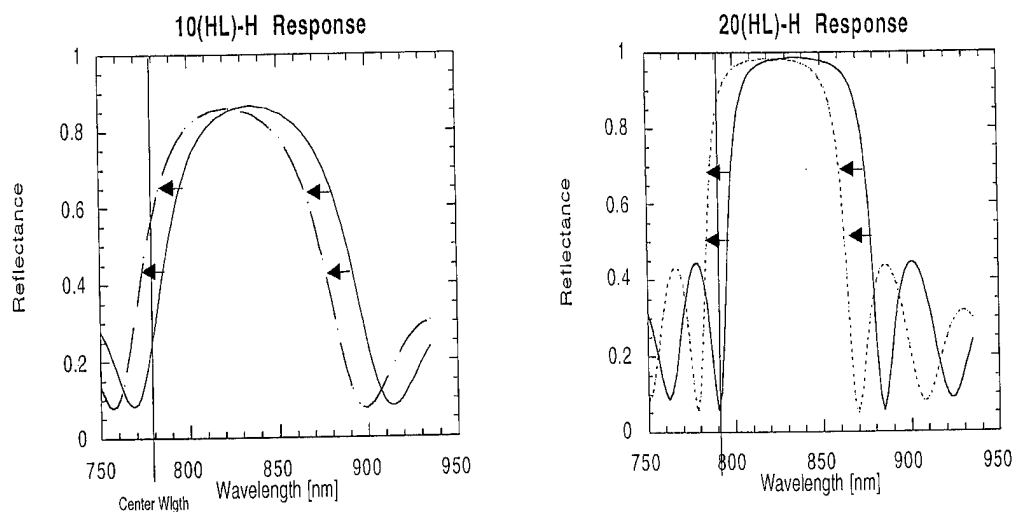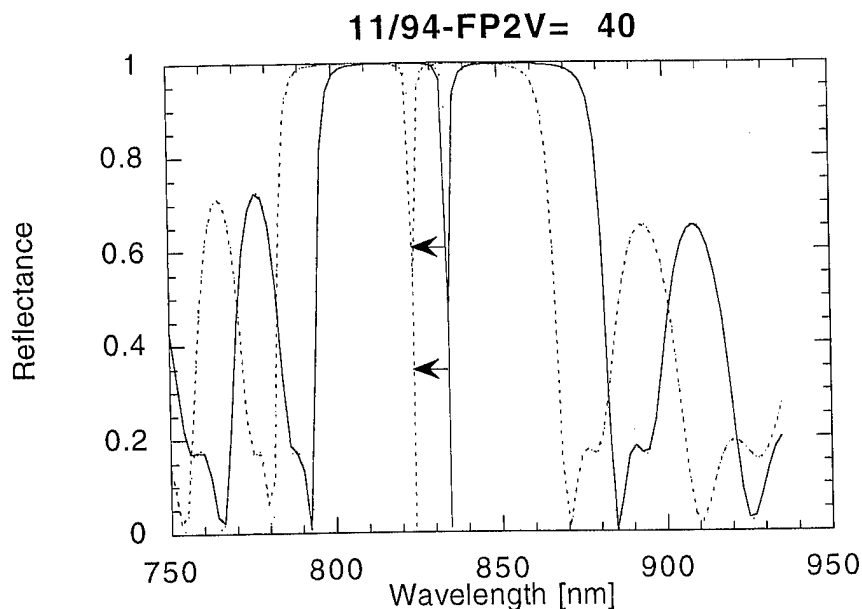Symmetric ferroelectric FP structures can also be used as tunable wavelength filters which can be controlled with electrical signals. Such device can be used to tune multi-line lasers or to perform wavelength de-multiplexing tasks. In general, FP filters are used as narrow band-pass filters to reject unwanted optical energy present in the vicinity of the center pass band as shown in Figure 3.3. If such a filter can be produced with ferroelectric layers, the narrow pass band can be shifted to different wavelengths. Thus, a ferroelectric FP filter can also be used as a wavelength tunable filter based on this principle.

The performance of both types of devices is mainly determined by the number of periods of alternating high/low index layers and the spacing of the electrodes. The steepness of the stop band and pass band edges increases as the number of periods in the stack increases. This dependence is demonstrated in Figsures 3.2(a) and 3.2(b). Moreover, an increase in the number of layers allows more desirable multilayer designs to be implemented. A typical multilayer FP filter consists of more than 40 pairs of alternating high/low quarter-wave optical thickness (or HL) layers with a roughly 2.10:1.45 index ratio. As the admittance, which determines the reflectance of the stack, depends approximately on this ratio raised to the number of pairs, using two materials with a lower index ratio requires a far greater number of pairs to achieve a similar performance. For example, to match the performance of 10 pairs of typical refractory materials with an index ratio of 1.45, using materials with, say, a 1.2 index ratio would require about 20 pairs to achieve comparable performance.

As the amount of spectral shift of ferroelectric multilayers is determined by the magnitude of the applied field, the electrode geometry that results in a maximum field should be utilized. The planar surface electrode is easiest to implement, but it requires the spacing, and thus the useful aperture, to be no greater than 15 μm wide. A previous study carried out at UCSD has demonstrated that a buried electrode configuration can give a 2 to 4 factor of increase in the field at the cost of a slight increase in capacitance. Longitudinal mode devices that utilize transparent indium tin oxide (ITO) electrodes would be most suitable for most applications as they would eliminate the limitation on the aperture size.

All of the following calculations assume average index and electro-optic coefficients from the values that were available. They are as follows:

High Index Layers:	n=2.618	r =1250 x 10^{-12} m/V
Low Index Layers:	n=2.337	r =1350 x 10^{-12} m/V
Substrate:	n=2.40	r = 420 x 10^{-12} m/V

3.3   Performance of Ferroelectric High Reflector (HR) Stack

The expected performances of ferroelectric HR stacks with different periods are summarized in the graph in Figure 3.4. For the transverse mode device, a surface electrode spacing of 10μm was assumed. For comparison, the expected responses of the same stack in the longitudinal mode are plotted. As the spectral curve shifts toward the shorter wavelengths in response to an applied field, the reflectance value of the stack at the design wavelength changes from near zero toward a maximum value close to unity with increasing voltage. The difference between the responses of stacks with different periods is due to the steepness of the edge of the stop-band which can be observed between Figures 3.2(a) and 3.2(b).

When 20 V is applied between 10 μm spaced electrodes, the reflectance rises to ~8% and ~60%, respectively, for 10 and 20 pair HR stacks. The benefit of exploiting the longitudinal electrode geometry is apparent. In this mode both stacks reach their near maximum modulation values at about 20 V. Even for less than 10 V, the calculations show that even a 10 pair stack can change from ~0% to >50% in reflectance.

HR Transverse (10μm) and Longitudinal SLM's
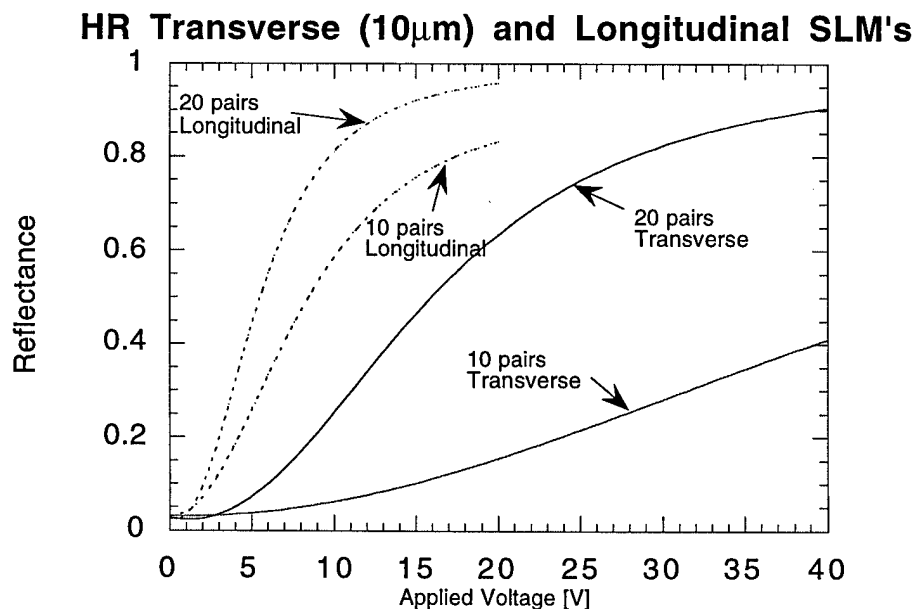

Figure 3.4 - Dependence of 10 pair and 20 pair HR stack reflectances on applied voltage. Transverse curves assume 10 μm surface electrode spacing. Note that longitudinal mode stacks result in more effect at less voltage due to the reduction of effective electrode spacing.

3.4 Performance of Ferroelectric Fabry-Perot (FP) Filter

Expected performances of a ferroelectric FP filter in transverse and longitudinal electrode configurations are summarized in the graph in Figure 3.5. For the transverse mode device, a surface electrode spacing of 10 µm was assumed as before. The FP filter design yields a better response at lower voltages, but it is much harder to make as the thickness of the layers needs to be controlled much more accurately. It is also more sensitive to incident angle deviations. Thus, it is much more suited to operate as a voltage tunable wavelength filter than as a spatial light modulator.

FP10/2/10-20V

Figure 3.5 - Dependence of reflectance of a 20-pair ferroelectric Fabry-Perot filter with full-wave spacer on applied voltage. Transverse curve assumes a 10 µm surface electrode spacing. Note that the longitudinal mode device outperforms transverse mode device.

3.5 Electro-Optic Thin Films for SLMs

The main objective for this task was to achieve high electro-optic response films operating at low voltages. For this task we selected PZT/PLZT, PBN:60 and SBN:75 because they possess outstanding electro-optic properties (Table 3.1) and because we expected that these materials could be made compatible with one other and with the selected substrates. The films are being grown using two techniques: sputtering and sol-gel. The results of our work using these methods have been briefly described below.

3.5.1 Single Layer Electro-Optic Films by the Sputtering Technique

We optimized the film growth conditions for PZT and SBN:75 on Pt-coated Si substrates, and found that highly grain-oriented films could be obtained when the substrate temperature was kept above 400°C during sputtered film growth. However, we could not achieve a remnant polarization above 15 $\mu C/cm^2$ in these films. In order to maintain low operating voltages in our stacks, we are currently depositing these films on lattice-matched SBN:60 substrates and the results of these experiments are promising. We have optimized the growth of PZT and SBN:75 films on SBN:60 substrates using the sol gel technique and because the film and substrate are lattice-matched, we could grow highly grain-oriented films. The results of our work on these two films are summarized below:

PZT Film	SBN:75 Film
- **Film thickness > 1 μm**	- **Film thickness > 1 μm**
- **Excellent surface quality**	- **Excellent surface quality**
- **Polarization > 38 $\mu C/cm^2$**	- **Polarization > 15 $\mu C/cm^2$**
- **r_{33} > 1000 x 10^{-12} m/V**	- **r_{33} > 700 x 10^{-12} m/V**

These films have been provided to UCSD researchers to analyze their performance for SLM applications.

3.5.2   Single Layer Electro-Optic Films by the Sol-Gel Technique

The sol-gel technique has been used to grow PZT thin films of two different compositions (52/48 and 60/40) on single crystal SBN:60, $LaAlO_3$ and metallized Si substrates. Stock solutions of each PZT composition were made using lead acetate, zirconium isopropoxide and titanium isopropoxide dissolved in 2-methoxyethanol. Just before deposition, the 0.6 M stock solution was diluted to 0.3 M with additional 2-methoxyethanol containing small amounts of water and nitric acid which act as hydrolyzers. The viscosity of the solution was such that a spin rate of 3000 rpm for 30 seconds resulted in ~650 Å of PZT deposition during each spin. In order to remove the organic components of the solution, it is necessary to heat the sample to 450 °C for a couple of minutes. By repeating the spin deposition process, PZT thin films of the desired thickness have been grown (1 to 1.5 μm).   We used both conventional and rapid thermal annealing (RTA) to crystallize the PZT thin films. However, we found that the RTA process produced PZT thin films

of desired quality and we continue to optimize the process for future work.

Excellent quality, highly grain-oriented PZT films of both compositions were obtained on SBN:60 and LaAlO$_3$ substrates. The lattice match between the selected PZT compositions and these substrates is excellent; hence, we expect to achieve high optical properties in these films. Figure 3.6 shows the x-ray diffraction pattern of a 0.75 μm thick PZT (60/40) deposited on SBN:60. Since the selected PZT composition and SBN:60 have a close lattice match, the crystallinity and grain orientation in the film are exceptional. Figure 3.7 shows the x-ray diffraction pattern of a PZT (60/40) thin film grown on LaAlO$_3$. From this data, it is readily apparent that the film is highly grain-oriented, but they are somewhat strained.

Figure 3.6 - X-ray diffraction pattern of a PZT (52/48) thin film on SBN:60.

Since for some applications we need PZT thin films on Si substrates, we studied extensively the grown of PZT films on Si. This requires Ti/Pt metallic layers on the Si substrates. The addition of these metallization layers also required the the RTA conditions be modified from those used in SBN:60 and LaAlO$_3$ depositions. However, the process has now been modified to grow PZT films on Si of excellent quality and thicknesses were maintained in the range of 0.5 to 1.5 μm. Figure 3.7 shows the x-ray diffraction pattern of a PZT (52/48) thin film on metallized Si. Since the films are not lattice matched with metallized Si, the films are typically polycrystalline when annealed over 700 °C.

Both of the PZT films are highly crystalline, so the measurement of the polarization and dielectric constant was possible. The results of our measurements are as follows:

- **Dielectric constant at room temperature : 1800 - 2000**

- **Spontaneous polarization : 18 - 20 $\mu C/cm^2$**

These properties are substantially higher and comparable to the values reported in the literature. Currently, we are in the process of improving the grain orientation in this films, so we can increase the polarization to > 28 $\mu C/cm^2$ in PZT. As discussed earlier, the spontaneous polarization in the range of 38 - 41 $\mu C/cm^2$ has been achieved in our highly oriented PZT films grown on SBN.

Figure 3.7 - X-ray diffraction pattern of PZT (60/40) thin film on $LaAlO_3$.

In order to effectively measure the dielectric characteristics of these PZT thin films, electrodes must be deposited above and below the film. Deposition of a metallization layer on SBN:60 or $LaAlO_3$ substrates would disrupt the lattice match and destroy the high grain orientation of the PZT films. In our previous work, we examined the use of $La_{0.5}Sr_{0.5}CoO_3$ (LSC) electrodes on various lattice-matched substrates for PZT deposition. Excellent grain orientation and high polarization (~30 $\mu C/cm^2$) was achieved using this system. However, standard metallization materials such as Ti/Pt and Cr/Au must be used with many MEMS applications in order to be

14

compatible with traditional processing techniques. Consequently, we have explored the use of Pt-metallized Si substrates for PZT thin film growth

Figure 3.8 shows an x-ray diffraction pattern of a 0.95 μm thick PZT thin film grown on Pt-metallized Si. As expected, the film is not grain oriented and shows the usual range of peaks with relative intensities seen in powder patterns. In addition to the Si [400] peak at 69°, two Pt peaks are seen at 39° [111] and 46° [002]. However, of more interest is the sharp, well-defined PZT peaks seen throughout the rest of the pattern. The PZT thin film is obviously well crystallized in the perovskite phase and shows no indication of the presence of any pyrochlore phase. This film was annealed at 675 °C for 2 minutes.

We are exploring the possibility of depositing a grain-oriented Pt metallization layer on Si substrates. If Pt can be grown with a [001]-type orientation, there are indications that grain-oriented PZT films could be deposited on this metallization layer. By varying the sputtering and post-deposition annealing conditions it may be possible to achieve the desired grain orientation in the Pt.
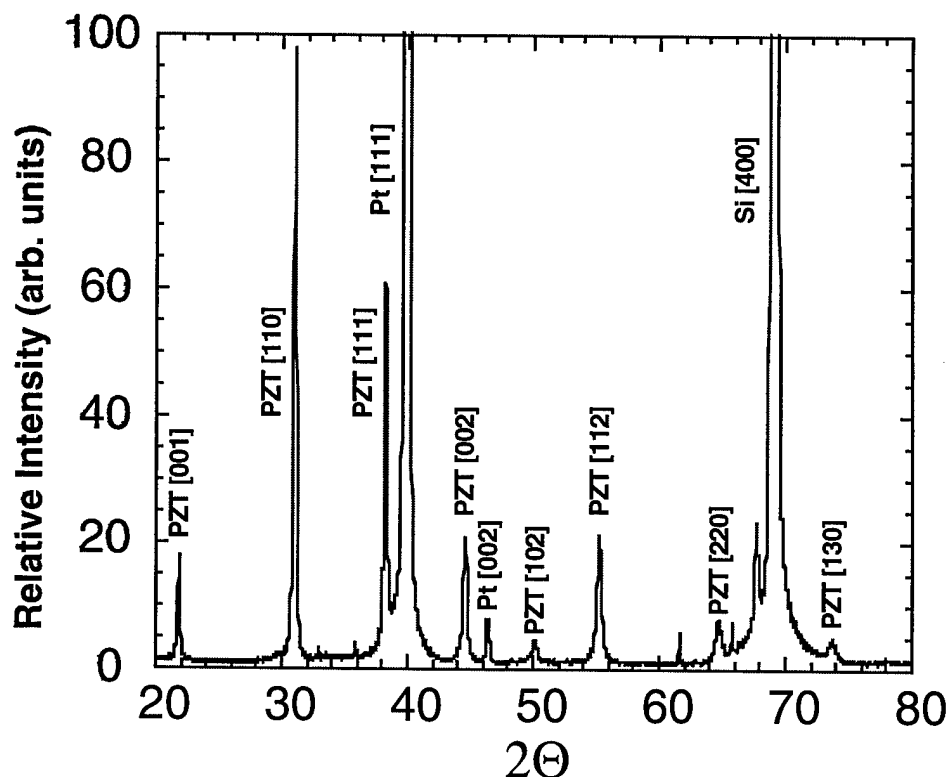

Figure 3.8 - X-ray diffraction pattern of PZT thin film on metallized Si substrate.

Some devices and substrates are temperature sensitive and not able to withstand the high annealing temperatures typically used to crystallize pyrochlore-free PZT thin films. One particular application we are beginning to explore is the use of PZT thin films for shape control in large inflatable space structures such as telescopes and antennas. In these applications, the substrate material is a durable plastic such as mylar or kapton which are not compatible with high annealing temperatures. Using Pt-metallized Si substrates, we have established the lowest temperature annealing conditions which produce pyrochlore-free PZT thin films.

Figure 3.9 shows a series of expanded x-ray diffraction patterns of 1.2 μm thick PZT thin films which were annealed at temperatures ranging from 500°C to 600°C. Two theta values of 20 to 35° were examined because they contain the perovskite PZT (100) and (110) reflections at 21.7° and 31°, respectively; in addition to the pyrochlore phase peak at 29.5°. This provides a convenient comparison of the relative amounts of the two phases. At 500°C annealing temperature, a significant amount of pyrochlore phase can be seen. However, as the temperature is increased the pyrochlore peak decreases until 600°C where no pyrochlore phase is detectable.
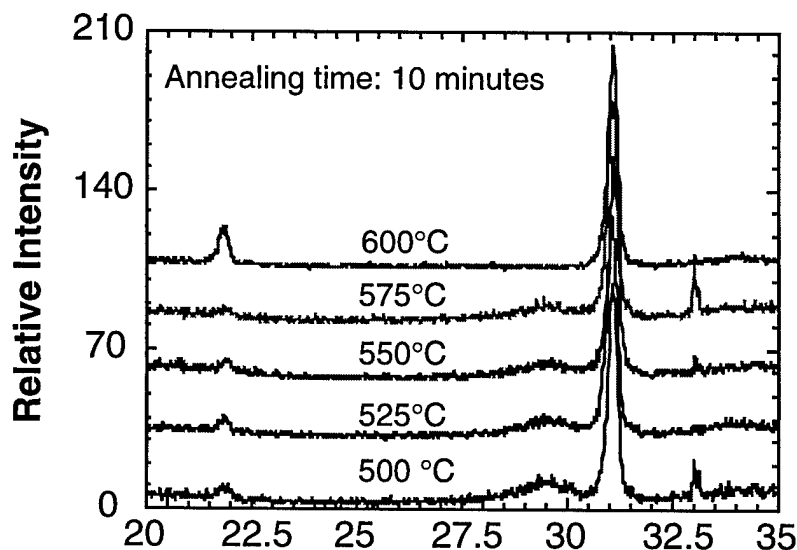

Figure 3.9 - Effect of annealing temperature on the formation of pyrochlore phase in PZT films.

Time is also an important parameter in the overall annealing conditions. We had hoped that by extending the annealing to longer times than is usually used for RTP, we might further reduce the temperature needed to avoid the formation of pyrochlore phase. Annealing times ranging from 1 to

10 minutes over the temperatures previously described were examined. As seen in Figure 3.9, pyrochlore formation was observed at temperatures below 600°C for the maximum annealing time of 10 minutes. Figure 3.10 shows the x-ray diffraction pattern of 1.2 μm thick PZT films annealed at 600 °C for times ranging from 2 to 10 minutes. As expected, a significant amount of pyrochlore phase was observed at shorter annealing times. Only a trace of pyrochlore phase is seen at 8 minutes annealing, but 10 minutes is required to produce pure perovskite phase. Figure 3.11 summarizes the results of the x-ray observations showing the amount of pyrochlore phase detected as a function of annealing time at 600°C.
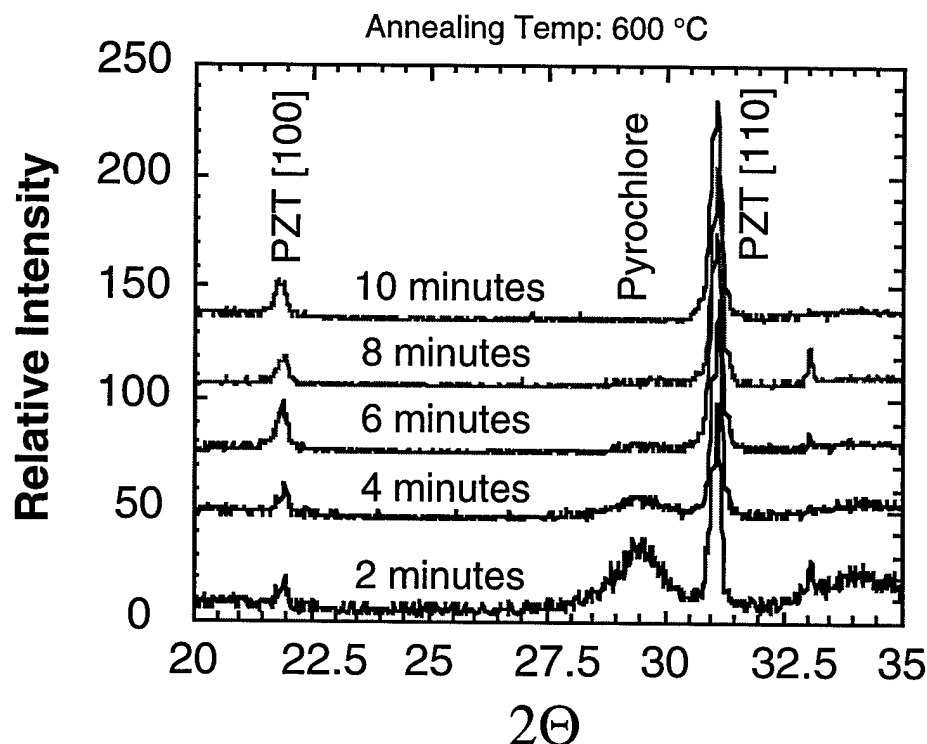
Figure 3.10 - Effect of annealing time on the formation of pyrochlore phase in PZT films.
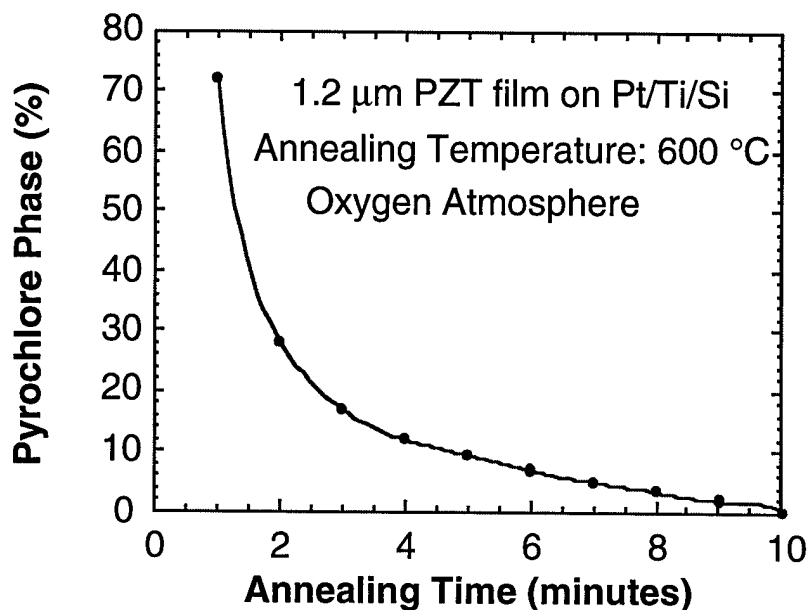
Figure 3.11 - Pyrochlore phase vs. annealing time for PZT film on metallized Si substrate.

3.5.3   Multilayer Films

The SLM structures in this program consist of ferroelectric perovskite PZT and tungsten bronze SBN:75 layers deposited on SBN:60 substrates (Fig. 3.9). Initially, we had utilized the sol-gel method for the deposition of PZT, followed by the sputter deposition of SBN for each pair of layers. Sputter deposition of SBN was utilized because of the difficulty of obtaining good sol-gel films of this highly refractory material. However, the smoothness of the sputtered SBN films was a major issue for these multilayer SLM stacks, particularly regarding the formation of island-type structures in the film which could seriously degrade the optical performance of the device.

Continuing work on SBN sol-gel formulations has now resulted in improved SBN films using this method. A critical issue was the ability to form (001) oriented SBN films on PZT, since unlike PZT which can have up to 14 possible directions for the polar axis, SBN has only two possible polar domain orientations along the c- axis. Figure 3.9 shows the x-ray diffraction results for a sol-gel SBN:75 film deposited on a PZT sol-gel film, with the underlying substrate being an optically polished SBN:60 single crystal plate. The diffraction data show only one dominant [002] peak, with the remaining peaks being greatly suppressed, as one would expect for a well-oriented

‹ Rockwell

Figure 3.12   Multilayer PZT and SBN:75 film structure grown on SBN substrate

film. The [001] peak is not prominent since it is not a strong diffraction peak in the SBN bronzes. Note that with the polar axis oriented normal to the plane of the film, a longitudinal SLM structure is the preferred configuration. The position of the [002] peak results in c-axis lattice constant of 3.913 Å, very close to the expected value of 3.921 Å found in single crystals. In the tetragonal a,b plane which interfaces with the PZT film, the expected a-axis lattice constant of 12.41 Å matches well with the tripled value of 12.24 - 12.30 Å for the near-cubic PZT lattice constant.

Figure 3.13 - X-ray diffraction pattern for SBN film on PZT.

A significant problem for the development of SLM stack structures has been the types of processing steps required when dealing with two entirely different material compositions. The methodology developed thus far involves an important alteration of the of the film annealing steps utilized as the stack is built up. Initially, $\lambda/4$ layers of first PZT (827 Å) and then SBN:75 (1037 Å) are deposited on the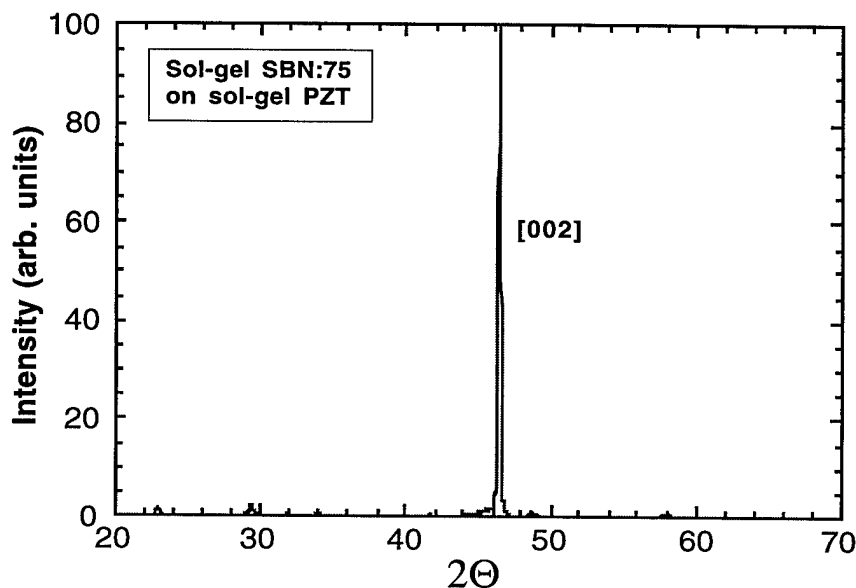 SBN:60 substrate, with each layer involving two high-speed spin depositions of the solution with an organic burn-out at 450 °C after each spin, followed by rapid thermal annealing (RTA) of the layer at 680 - 720 °C for 15 seconds. This same procedure is utilized for the second PZT layer deposited on the SBN film. From this point on for the remaining film layers, the same solution spin-on and burnout procedures are retained, but the film annealing step is performed after the deposition of (SBN + PZT) layer pairs. Stacks up to sixteen layer pairs have now been successfully grown in this manner.

The rapid thermal annealing procedure utilized for these multilayer stacks has shown smoother film morphology than for other methods, while still retaining the lattice orientation for the critical SBN film layers as well as for the PZT layers. In contrast, long-term furnace anneals (typically, 0.5 hour) at lower temperatures have generally resulted in poorer film morphology, as well as film peeling in the case of stacks with several deposited layers.

PZT + SBN:75 layer pairs have shown good hysteresis (polarization vs. electric field), albeit with lower than desired remnant polarization values. An example of the ferroelectric hysteresis for one such layer pair is shown in Fig. 3.10, in which $P_r = 4.5$ μcoulombs/cm^2, substantially lower than the 15 - 20 μC/cm^2 minimum value expected. Film stress may play an important role here, a feature which can be at least partially overcome by alterations of the film composition. Since, in particular, the phase transition for SBN:75 crystals occurs close to room temperature (48 - 54 °C), any broadening of the ferroelectric phase transition region due to stress and/or nonuniformities can have a serious negative impact on the ferroelectric properties of the SBN film. This has been observed, for example, in single-layer SBN films in which the transition region was considerably broadened as well as moved to near room temperature, resulting in reduced remanent polarization [6]. This problem would not be expected to have as much impact on the PZT films since their transition temperatures are 200 °C or more above room temperature, depending upon the final film composition.

These issues are now being addressed in continuing work. This includes examining the possible need for tighter control over the orientation of the SBN:60 substrates. Certainly any substrate misorientation (1° or more) will result in decreased photorefractive properties in the thin films. Hence, we are working to improve our substrate processing to insure a high degree of proper substrate orientation prior to film deposition.
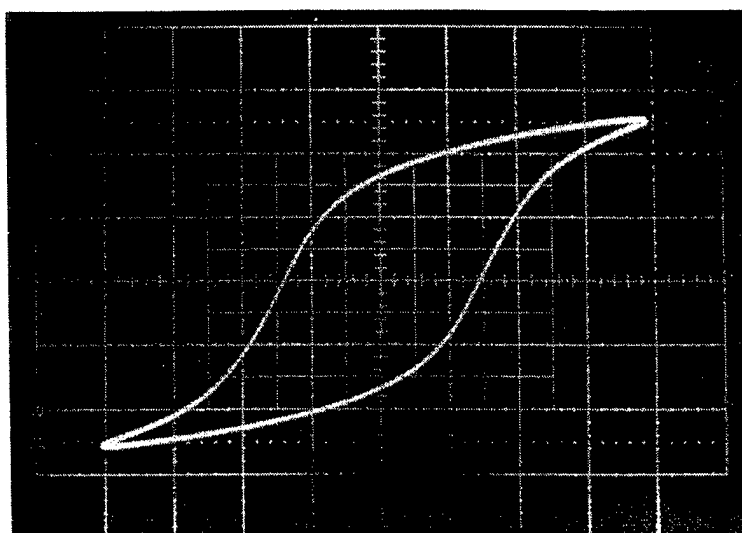

Figure 3.14 - Hysteresis loop for a PZT/SBN layer pair.

3.5.4   Ferroelectric Multilayer Optical Characterization

Two ferroelectric multilayer HR samples from Rockwell were evaluated. They consisted of 8 and 16 pairs of alternating PZT/SBN:75 quarter-wave optical thickness layers deposited on SBN:60 substrates. A maximum transmittance of the stacks of about 90% was obtained at 633 nm, indicating very high optical quality thin films constituents. Square aluminum surface electrodes of different sizes were deposited on both samples. The electrode spacing varies from 5 to 40 μm. Preliminary measurements made with a random laser source (633 nm He-Ne) did not indicate any electro-optic response, as expected, due to the lack of spectral response information. In order to observe the maximum electro-optic effect, the wavelength where the reflectance minimum is closest to the stop-band on the shorter wavelength side needs to be determined through wavelength spectrum measurements. We plan to carry out this task in the near future and repeat the electro-optic measurements at the appropriate wavelength.

The optical measurements on these stacks showed substantial increase in modulation depth suggesting the concept of stacking alternate PZT and SBN layers is a viable approach. We continue to improve the properties and quality of these films, so we can achieve maximum modulation, which is required for various SLM applications. Our recommendation for future work are as follows:

1.   Improve the film quality and achieve complete poling.
2.   Optimize modulation vs number of PZT/SBN layers.
3.   Other film layers in the place of SBN:75. Since SBN:75 requires higher annealing temperatures, it is important to identify suitable films compositions that can be annealed at relatively lower temperatures.

4.0 PHOTOREFRACTIVE FILMS

For photorefractive applications, one needs highly grain-oriented films, doped with suitable dopant(s), where no electric field is required to utilize the photorefractive effect. Since SBN has an excellent lattice-match with both PZT and BaTiO3, we have exploited SBN as a substrate material for the growth of these high optical figure-of-merit films. The films have been grown by the sol-gel technique and the details of their growth are as follows:

Film Composition:	PZT and $BaTiO_3$
Substrate:	[001]-oriented SBN:60 & SBN:50, [100]-oriented $SrTiO_3$ and MgO.
Dopants:	Fe^{2+}/Fe^{3+} or Ce^{3+}/Ce^{4+}
Annealing Temperature:	600 - 700°C for PZT films 750 - 800°C for $BaTiO_3$
Film Thickness:	2 - 3 μm for PZT 3 - 5μm for $BaTiO_3$
Photorefractive Properties:	Fast response and high coupling

4.1 Photorefractive PZT Films

Table 3.2 has previously summarizes the growth conditions for the PZT films and the results of each growth in terms of film thickness and the degree of orientation. The most extensive set of growth experiments was carried out on SBN substrates. These included two different substrate orientations with no buffer layer and conducting LSC buffer layer. The conducting buffer layer allows direct measurements of the ferroelectric properties of the PZT films.

As shown by the x-ray diffraction patterns in Figure 4.1, the PZT films deposited on [001] SBN:60 substrates are highly oriented along the [100] direction of the perovskite structure because of the close lattice match between [100] PZT and [001] SBN:60. This is the first time the sol-gel

process has been successfully used to grow highly grain-oriented PZT films on SBN. Since the refractive index difference between PZT and SBN:60 is large ($\Delta n \sim 0.218$), this structure could have a significant impact on photorefractive and electro-optic applications. We are currently adjusting the film composition to improve the lattice match with SBN:60, which will lead to lower strain and fewer defects in the films. In contrast, PZT films grown on [100]-oriented SBN:60 substrates are typically lattice-mismatched and therefore the films are polycrystalline with no preferred orientation.

Also shown in Figure 4.1 is the diffraction pattern for PZT grown on SBN/LSC. The LSC buffer layer grows on SBN:60 as a highly oriented cubic perovskite with a lattice constant slightly lower than the c-axis value for SBN. For this reason, the subsequent PZT layer also achieves good grain orientation.

Figure 4.2 shows the x-ray diffraction patterns for grain-oriented PZT films on LSC coated $SrTiO_3$ and MgO substrates. Since the film, substrate and buffer layers are all perovskite, we expected that the crystallinity of the PZT films on $SrTiO_3$/LSC should be good. It has been reported that single crystal PZT films have been grown by rf sputtering on [100]-oriented $SrTiO_3$ substrates for optical applications, but this is the first instance of sol-gel growth of such films. Efforts are under way to study the film quality for optical applications using [110] and [111]-oriented $SrTiO_3$ substrates.

Photorefractive measurements on our Fe and Ce-doped PZT films indicate that the films are strongly photorefractive and their properties can be modified according to our needs. The photorefractive response in these films is not sufficiently fast, indicting that the doping concentration in these films is insufficient or is nonuniform. In our future growth studies, we plan to address these issues and reexamine these films with respect our proposed device concepts. Our current results are:

- Polarization: $> 30\ \mu C/cm^2$ (in highly oriented films)

- Photorefractive response: $\sim 100\ ms$

We have also grown (100)-oriented Fe-doped $BaTiO_3$ thin films on SBN:60 and the results of our work are promising. Since $BaTiO_3$ is highly refractory material, it requires higher annealing temperatures ($> 800°C$) compared to PZT films. Detailed information on this system will be provided in our next report.
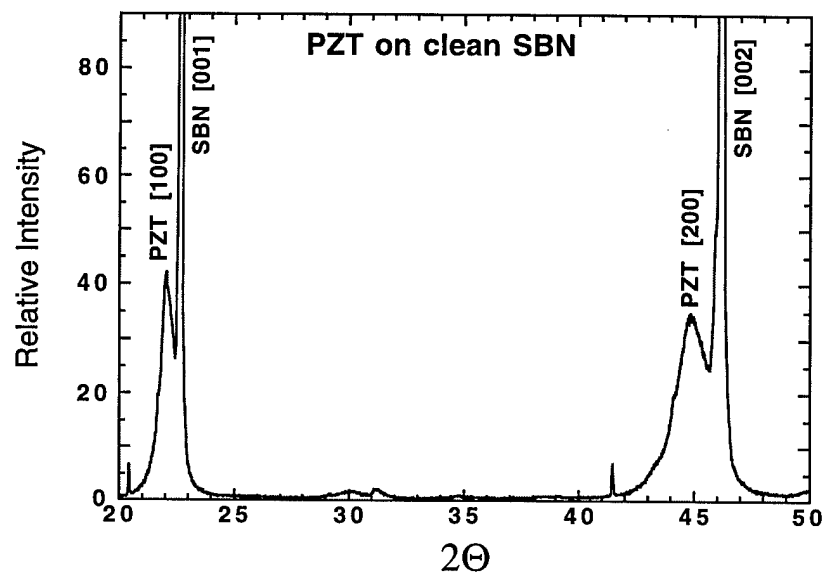
Figure 4.1(a) - X-ray diffraction pattern of a PZT film on clean SBN substrate.
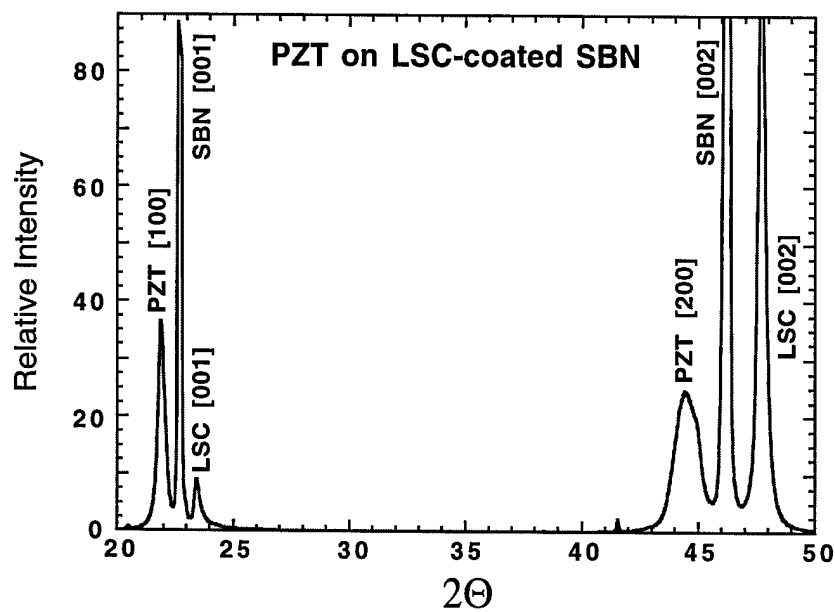

Figure 4.1(b) - X-ray diffraction pattern of a PZT film on LSC-coated SBN substrate.
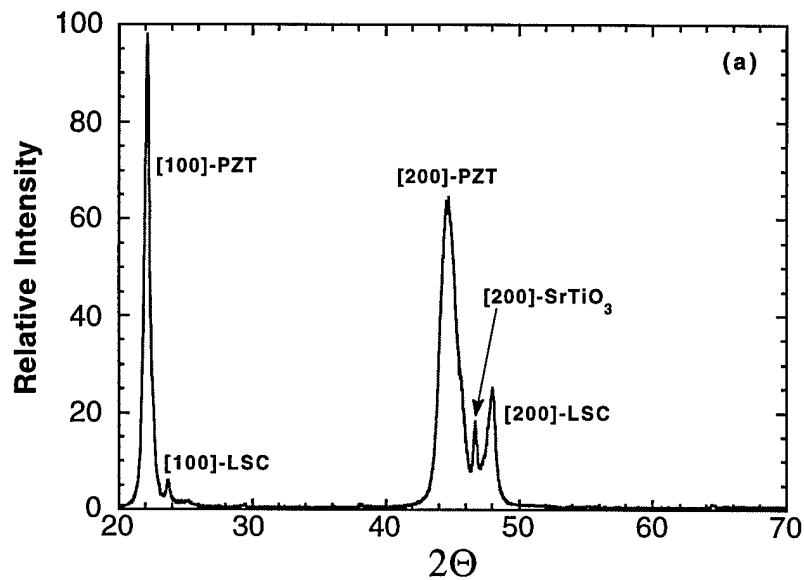
Rockwell

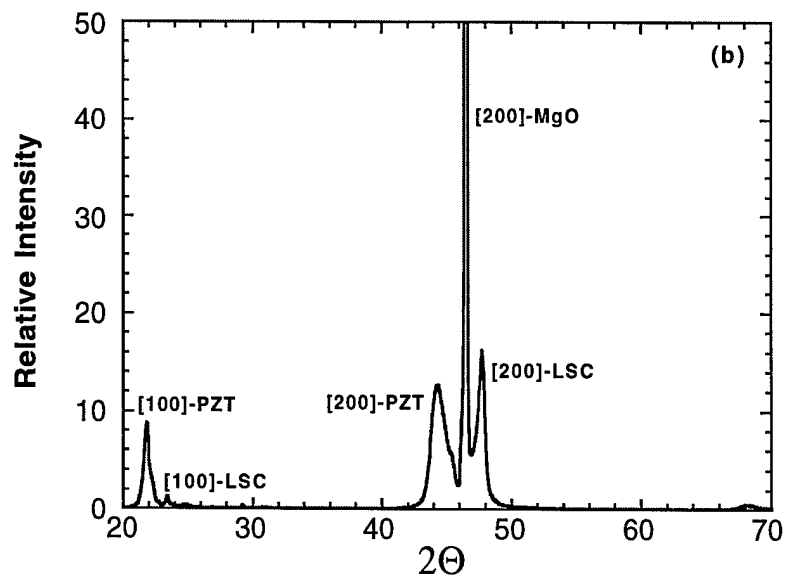Figure 4.2(a) - X-ray diffraction pattern of a PZT film on SrTiO$_3$ with LSC layers.

Figure 4.2(b) - X-ray diffraction pattern a PZT film on MgO with LSC layers.

4.2 Growth of Tungsten Bronze Pb^{2+}-Containing Thin Films

During this program , we have also grown PSKNN thin films with the tungsten bronze structure. The PSKNN compositions are based on the $Pb_2KNb_5O_{15}$- $Sr_2NaNb_5O_{15}$ (PSKNN) morphotropic phase boundary system and they exhibit excellent ferroelectric and optical properties. This solid solution lies of two orthorhombic tungsten bronze compositions $Pb_2KNb_5O_{15}$ and $Sr_2NaNb_5O_{15}$, the first of which has a polar axis along [100] or [010] direction, while in the latter polar axis is strictly along the [001] direction. In the present work, we selected composition closer to MPB region on the $Sr_2NaNb_5O_{15}$ side and have grown the films on SBN:60 substrate with significant success.

Since the lattice match between SBN:60 and PSKNN is very close, the quality of PSKNN films was generally excellent. Consequently, the polarization obtained in these films is closer to expected range (~ 30 $\mu C/cm^2$) , giving rise to high electro-optic coefficients (r_{ij}). A detailed account of this work has been provided in Appendix .

Recently, we have demonstrated the switching of the polar axis from [001] to [100] in PSKNN films on the application of an external electric field of ~ 2 kV/cm. As mentioned elsewhere in this report, this effect is important for optical switching applications, and this will open up new applications for these films.

5.0 Recommendation

This program has been sucessful in producing the highest polarization in ferroelectric PZT films to date. This progress illustrates the potential for developing practical photorefractive and guided-wave devices based on PZT and other morphotropic phase boundary (MPB) thin films. The improvement in optical figures-of-merit (r_{ij}/ε) in our work is illustrated in Figure 5.1. Currently, $LiNbO_3$ is the primary material used in most applications, because it is commercially grown in large size and optical quality. However, $LiNbO_3$ based devices require high operating voltages and large sizes.

Established Materials

Products commercially
available (Bulks + Films)

OPTICAL PRODUCTS

- $LiNbO_3$ & $LiTaO_3$
- KDP & ADP

$r_{ij}/\varepsilon \sim 0.5$

Order of Magnitude Better

Current Materials

- T.B.   BSTN, BSKNN
- Perovskites: KTN, $BaTiO_3$

$r_{ij}/\varepsilon \sim 0.8$

- Switchable Polarization
- Easy to Pole
- Low Switching Energy

FUTURE MATERIALS

- MPB THIN FILMS
  (PZT, PBN, PBKNN)

$r_{ij}/\varepsilon > 1.5$

Figure 5.1 Illustrates optical figure-of-merit for various materials

On a related program, we have developed tungsten bronze crystals exhibiting higher figure-of-merit materials and these crystals are being exploited in various new photorefractive and guided-wave optical structures. PZT and other MPB thin films offer even greater figure-of-merit and therefore are potentially superior in these applications. Therefore, these material systems should be

28

further developed specifically for guided-wave optical applications and later for photorefractive applications, where the role of dopants will need to be optimized.

The MPB systems of most interest for future development are shown in Figure 5.2 and 5.3. On a simple binary phase diagram, an MPB appears as a nearly vertical line separating two ferroelectric phases, i.e., the boundary occurs at a nearly constant composition over a wide temperature range up to the Curie point. Poled crystals near the MPB show unique and enhanced ferroelectric and optical properties because of the proximity in free energy of an alternate ferroelectric structure.

Figure 5.2 --Composition-temperature phase diagram for PZT system.

In the MPB region, one can switch the polar axis from [100] to [001] or vice versa by the application of an electric field, which provides a new mechanism to accomplish optical switching. Both PZT and PBN are promising systems and they will provide all these features in thin films. Recently, at the Rockwell Science Center, we have identified and established over 10 new MPB systems and some of them are potentially useful for optical applications.

Figure 3.3 - Composition-temperature diagram for PBN system.

Table 5.1

Summary of a Few Tungsten Bronze and Perovskite MPB Systems

System	x at MPB	Phases	T_c (°C)
		at MPB	at MPB
Tungsten Bronze Systems			
$PbNb_2O_6$-$BaNb_2O_6$ (PBN)	0.37	Ortho-Tetra	300
$Pb_2KNb_5O_{15}$-$Sr_2NaNb_5O_{15}$ (PSKNN)	0.70	Ortho-Ortho	145
$Pb_2KNb_5O_{15}$-$Ba_2NaNb_5O_{15}$	0.25	Ortho-Ortho	255
Perovskite Systems			
$PbZrO_3$-$PbTiO_3$ (PZT)	0.48	Rhombo-Tetra	360
$PbTiO_3$-$BiFeO_3$ (PTBF)	0.40	Tetra-Ortho	450
$PbTiO_3$-$PbSnO_3$ (PTSn)	0.45	Tetra-Rhombo	250

Table 5.1 summarizes various MPB systems based on the tungsten bronze and perovskite structures. The most commonly known MPB systems from these families are PBN and PZT, respectively. We have identified many systems within the tungsten bronze family and further study is required to establish their importance for optical and other applications. Since the bulk crystal growth of Pb^{2+} -containing compositions is generally difficult, the thin film growth of these systems is an appropriate alternative.

Table 5.2 summarizes various applications using high performance ferroelectric thin films and their associated advantages in each application area. Currently, ferroelectric films are also explored for electronic memory applications, and achieving switchable polarization is a key issue. Besides PZT thin films, various films are being considered and most of them do not meet all the requirements. The tungsten bronze ferroelectric thin films offer a major advantage for these applications and can be further developed according to device requirements.

Table 5.2
Applications and Selected Film Structures

Applications	Current Film Structures	Proposed Film Structures	Advantages
SLM's - Interconnects	Stack: PZT-SBN:75	Stack: PZT-PSKNN Stack: PZT-PTBF	High modulation Operation at low voltages
Photorefractive - Pattern Recognition - Image Processing - 3-D memory & Storage	$BaTiO_3$ & SBN:60	PZT	High space charge Fast speed & high diffraction efficiency
Guided-Wave Optics - Telecommunication - Signal processing - Switches & Filters	$LiNbO_3$	PSKNN	Operation at low voltages High frequency range Low optical Loss
Electronic memory - F-Ram & D-Ram	PZT	PSKNN	Easy to switch polar axis

All film compositions selected are close to MPB region

31

6.0   REFERENCES

1. J. Neff, R. Athale and S. H. Lee, Proceedings of the IEEE **78** (5), 826 (1990).

2. A. Fisher,   International Journal of Optoelectronics **5** (2), 125 (1990).

3. S.   Esener, A. Krishnamoorthy, S. H. Lee, "Optoelectronic Tecnology for Neural Networks", to be published by Academic Press.

4. S. H. Lee, Opt. Eng. **25** (1), 69 (1986).

5. M. S. Jin, J. H. Wang V. H. Ozguz, and S. H. Lee, Appl. Op.t **33** (14), 2842 (1994).

6. R.R. Neurgaonkar, I.S. Santha and J.R. Oliver, Mat. Res. Bull. **26**, 771 (1991).

7.1   APPENDIX

Ferroelectric Thin Films and Their Applications

Appendix 7.2

Grain Oriented Ferroelectric PZT Thin Films on Lattice-Matched Substrates

FERROELECTRIC THIN FILMS AND THEIR APPLICATIONS

R. R. Neurgaonkar, J. R. Oliver, J. G. Nelson and I. S. Santha
Rockwell Science Center
Thousand Oaks, CA 91360

ABSTRACT

Ferroelectric morphotropic phase boundary (MPB) materials based on Pb^{2+} - containing compositions are potentially important for optical and electronic applications because they exhibit high switchable polarization near this boundary with superior electro-optic and piezoelectric properties. In this paper we discuss these MPB materials, substrate issues, and the growth of MPB film compositions based on the PZT and PSKNN systems.

INTRODUCTION

Guided-wave electro-optic devices are widely used with optical fibers for applications in communications, signal processing, sensing and spatial light modulators [1,2]. The realization of low-loss single mode optical waveguides is critical to the practical implementation of these devices, and it is desirable to use materials with large electro-optic coefficients to achieve low voltage performance. Ferroelectric oxide crystals have generally been a popular material choice for this technology. The most widely used among these have been $LiNbO_3$ and $LiTaO_3$ crystals or films in the ilmenite family, primarily because of their commercial availability and established methods for fabricating optical waveguides in each case [3-6]. Significant interest, however, lies in producing optical waveguide devices in other ferroelectric materials with higher electro-optic coefficients which could be used for making compact, low-voltage electro-optic modulators and switches, as well as tunable wide-band filters. Recently, Taylor and Eknoyan (7-10) did extensive work on the tungsten bronze materials and reported that these ferroelectrics (SBN, BSTN, BSKNN, KLN, BNN) provide an attractive choice for such needs because their linear electro-optic coefficient (r_{33}) is generally much greater in magnitude than that in $LiNbO_3$ and $LiTaO_3$. At Rockwell, we have identified several morphotropic phase boundary (MPB) materials based on Pb^{2+}-containing systems in which polarization is exceptionally large near such regions, thus giving large electro-optic (r_{ij}) and piezoelectric (d_{ij}) coefficients. Although the single crystal growth work on these materials has been frustrated due to the loss of Pb^{2+} during the growth, we have been successful in fabricating good quality films with high optical figures-of-merit. In this paper, we describe our thin film work on perovskite PZT and tungsten

bronze $Pb_{2-x}Sr_xK_{1-y}Na_yNb_5O_{15}$ (PSKNN), with emphasis on current useful substrate materials.

EXPERIMENTAL PROCEDURE

PZT and PSKNN thin films were fabricated using the sputtering and sol-gel techniques. The sputtering targets employed were a mixture of PZT or tungsten bronze PSKNN and PbO. Approximately 5 mole% excess PbO was added in the targets to control the Pb^{2+} concentration in the films. The targets were prepared using ceramic sintering; well-mixed powders were cold pressed and then sintered at 1000 °C after ball-milling.

The sputtered PZT and PSKNN thin films were deposited with an MRC rf sputtering instrument; the sputtering conditions are summarized in Table 1. SBN:60 and $LaAlO_3$ crystals of dimensions 10 x 10 x 1 mm were cut in the [001] plane. Some of the substrates were polished to optical quality, etched with HF acid after polishing, or mechanochemically polished. The substrate temperature was maintained between 200-500 °C during these film depositions.

The procedure followed for preparation of the sol-gel solutions has been outlined by Udaykumar et al.[11] using Pb^{2+}- acetate trihydrate, Ti^{4+}-iso-propoxide and Zr^{4+}-n-propoxide solutions. The concentration of each solution was adjusted to 1M by either the removal or addition of 2-methoxyethanol. The thin film growth procedures and annealing conditions are discussed in earlier papers [12,13].

The phase purity and grain orientation of the films were characterized by x-ray diffraction techniques. For ferroelectric measurements, platinum or $La_{0.5}Sr_{0.5}CoO_3$ (LSC) electrodes were used. The dielectric constant and dielectric loss tangent of the films were measured as a function of temperature and frequency using a multifrequency LCR meter. The polarization-field (P-E) hysteresis loop and fatigue life were measured using modified Sawyer-Tower circuit at 23 °C.

RESULTS AND DISCUSSION

Morphotropic Phase Boundary Systems

The search for increased electro-optic and piezoelectric effects in ferroelectric crystal families has stimulated interest in a number of potential morphotropic phase boundary (MPB) systems.

On a binary phase diagram, an MPB appears as a nearly vertical line separating two distinct ferroelectric phases. This phase boundary generally occurs as a nearly constant composition over a wide temperature range up to the ferroelectric phase transition temperature, T_c, an example is shown in Figure 1 for the well-known tungsten bronze MPB system $Pb_{1-x}Ba_xNb_2O_6$ (PBN), which possesses both orthorhombic and tetragonal structures near $x = 0.37$ [10-13]. Poled thin films or single crystals of such MPB ferroelectrics can show an enhancement of numerous physical properties because of the proximity in free energy of an alternate ferroelectric structure; detailed descriptions of MPB behavior can be found in the work by Jaffe et al [14].
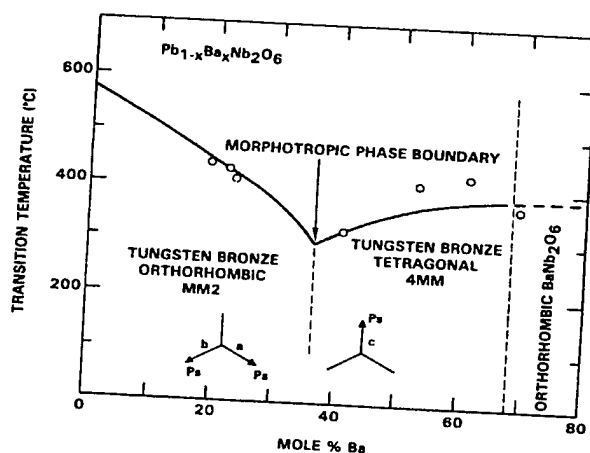

Figure 1 - Phase diagram for the $Pb_{1-x}Ba_xNb_2O_6$ MPB system.

The PBN solid solution is based on the binary system $(1-x)PbNb_2O_6$ - $(x)BaNb_2O_6$, as shown in Figure 1. The crossover between the Curie temperatures Θ_1 and Θ_3 as one moves the composition through the MPB region leads to very large electro-optic and piezoelectric constants at room temperature, in spite of the high ferroelectric phase transition temperature. For example, tetragonal PBN:60 has dielectric constant $\varepsilon_{11} = 1900$ along the a axis and $\varepsilon_{33} = 500$ along the c axis. The spontaneous polarization in poled crystals is also large, in the range of 50-60 $\mu C/cm^2$ at room temperature based on the Penn State measurements [15,16].

The large spontaneous polarization and large dielectric constants available in PBN are especially significant for optical applications. From the phenomenology for oxide ferroelectrics [17], the linear electro-optic effect may be considered a quadratic effect biased by the nonzero spontaneous polarization in the ferroelectric phase. In the case of the tetragonal tungsten bronzes,

the linear electro-optic coefficients, r_{ij}, are given by relations of the form [17]

$$r_{13} = 2g_{13}P_3\varepsilon_{33}\varepsilon_o$$
$$r_{33} = 2g_{33}P_3\varepsilon_{33}\varepsilon_o$$
$$r_{51} = r_{42} = g_{44}P_3\varepsilon_{11}\varepsilon_o, \tag{1}$$
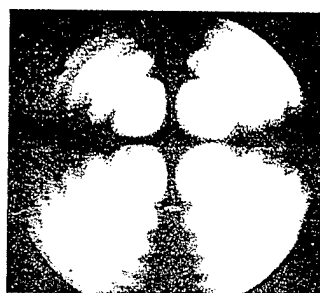
where P_3 is the c-axis polarization and the g_{ij} are the quadratic electro-optic coefficients, with the latter being taken as largely independent of temperature with values roughly the same as those in the high-temperature paraelectric phase. Similar relations also apply for the piezoelectric d_{ij} coefficients, with the quadratic g coefficients being replaced by Q_{kl} electrostriction constants. Recently, we have demonstrated using our optical quality crystals that $g_{ij} > 2.4\,Q_{kl}$ in these materials [18]. Furthermore, the evaluation of d_{ij} is much simpler than measurements of r_{ij}; using these d_{ij} values we can easily estimate the r_{ij} for a given MPB material.

The relation for r_{51} in equation (1) is of particular interest in that for tetragonal compositions near MPB, but far from the ferroelectric transition temperature, both P_3 and ε_{11} can be large and nearly independent of temperature. In the case of single crystal PBN:60, r_{51} is now estimated at greater than 2000×10^{-12} m/V at room temperature, many times greater than the values for the best non-MPB materials. For orthorhombic (mm2) compositions near an MPB with the polar axis along **a (or b)**, the equivalent relations are given by

$$r_{11} = 2g_{11}P_1\varepsilon_{11}\varepsilon_o$$
$$r_{12} = 2g_{12}P_1\varepsilon_{11}\varepsilon_o$$
$$r_{13} = 2g_{13}P_1\varepsilon_{33}\varepsilon_o$$
$$r_{43} = g_{44}P_1\varepsilon_{33}\varepsilon_o.$$

In this case P_1 and ε_{33} can be large, so that large and nearly temperature-independent values of r_{13} and r_{43} may be anticipated. We have successfully demonstrated in PBN crystals that if the composition is very close to MPB region, the polar axis is easily switched from P_3 to P_1, as shown in Figure 2, or vice versa. This behavior can be used as a switching mechanism for various optical and piezoelectric applications.

Table 1 summarizes various MPB systems based on the tungsten bronze and perovskite structures. The most commonly known MPB systems from these families are PBN and PZT, respectively. We have identified many systems within the tungsten bronze family; further study is required to establish their importance for optical and other applications. Since the bulk crystal growth of Pb^{2+}-containing compositions is difficult, the thin film growth of these systems is an appropriate alternative.

| (a) | (b) |

Figure 2 - Switching of polar axis in PBN:60 crystal under an external electric field: (a) PBN:60 tetragonal uniaxial interference E = 0 and (b) PBN:60 orthorhombic interference after E = 20 kV/cm applied in [110] direction.

Table 1
Summary of a Few Tungsten Bronze and Perovskite MPB Systems

System	x at MPB	Phases at MPB	T_c (°C) at MPB
Tungsten Bronze Systems			
$PbNb_2O_6$-$BaNb_2O_6$ (PBN)	0.37	orthorhombic-tetragonal	280
$Pb_2KNb_5O_{15}$- $Sr_2NaNb_5O_{15}$ (PSKNN)	0.70	orthorhombic -orthorhombic	145
$Pb_2KNb_5O_{15}$- $Ba_2NaNb_5O_{15}$ (PBKNN)	0.25	orthorhombic-orthorhombic	255
Perovskite Systems			
$PbZrO_3$ - $PbTiO_3$ (PZT)	0.48	rhombohedral -tetragonal	360
$PbTiO_3$ - $BiFeO_3$ (PTBF)	0.40	tetragonal-orthorhombic	450
$PbTiO_3$ - $PbSnO_3$ (PTSn)	0.45	tetragonal-rhombohedral	250

Growth of PZT and PSKNN Thin Films

In this laboratory work has focused on potential optical applications of ferroelectric thin films including guided-wave optics, photorefractive and spatial light modulator (SLM) devices. For this reason, we selected high electro-optic (r_{ij}) coefficient materials PZT and PSKNN, which need to be grown with good optical quality for these applications. In order to achieve this, a good lattice match with the substrate is essential, and film orientation must be properly maintained. If these conditions are met, grain orientation in the films is of high order and yields high r_{ij} with low optical losses.

Table 2 summarizes a number of substrates being used for the growth of ferroelectric thin films. Since optical applications require single crystal or highly oriented thin films, we employed lattice-matched perovskite $LaAlO_3$, cubic $NdGaO_3$ and tungsten bronze SBN:60 single crystal substrates. These substrates are being grown at Rockwell in optical quality and large sizes (~ 6 cm diameter). With these substrates, we have been successful in growing highly oriented thin films.

Table 2
Substrate Base for Ferroelectric Thin Film Development

Semiconductor	Paraelectric: Lattice-Matched
Si, GaAs, Ge	$SrTiO_3$, $KTaO_3$, $BaTiO_3$
	$KMnO_3$, $KMgO_3$
	$LaAlO_3$, $NdGaO_3$, $NdAlO_3$
Non-Ferroelectric	Ferroelectric: Lattice-Matched
MgO, Al_2O_3	SBN, BSKNN, SCNN
ZrO_2, $MgAl_2O_4$	$LiNbO_3$, $LiTaO_3$

As shown in Figures 3 - 6, highly oriented and single crystal films of PZT and PSKNN have been grown by both sputtering and sol-gel techniques. The x-ray diffraction patterns provided here are for sol-gel films which exhibit excellent crystallinity. In the case of sputtered deposition, annealing may not be necessary if the substrate temperature is maintained over 450°C for both PZT (c = 3.998 Å) and PSKNN (c = 3.956 Å) films. For the sol-gel films, annealing was carried out in the temperature range of 500-700 °C to achieve good crystallinity. PZT has a lattice-match with [001] oriented SBN, and we grew only these films with and without LSC

electrodes. In the case of PSKNN, we have grown films on SBN:60 in three different orientations, namely, [001], [100] and [111], with excellent crystallinity and film quality. Figures 5 and 6 show [001] and [100]-oriented PSKNN films on SBN:60 substrates. Both the PZT and PSKNN films have been grown as thick as 5 μm.
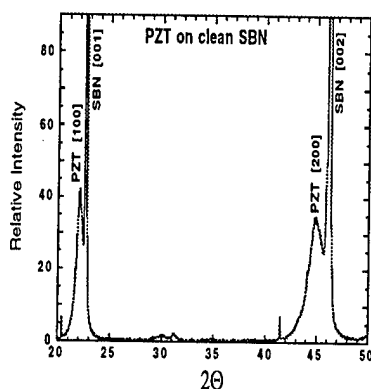

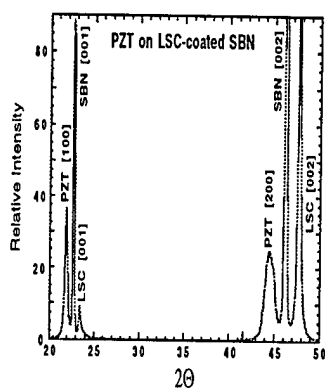
Figure 3 - PZT film on SBN:60.
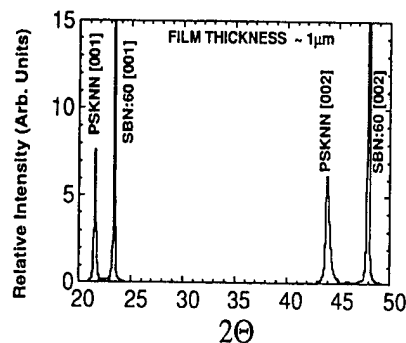

Figure 4 - PZT film on LSC/SBN:60.
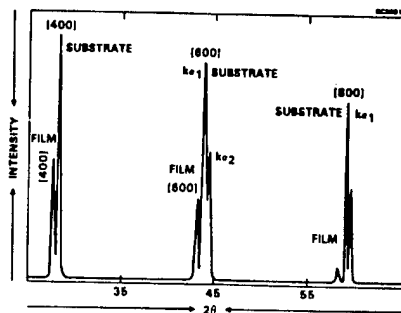

Figure 5 - PSKNN Film on [001] SBN:60.

Figure 6 - PSKNN Film on [100]SBN:60.

Electrical measurements were carried out using platinum surface contact pads of either 0.00485 cm^2 or 0.0182 cm^2 area sputtered onto the film surface. The substrate electrode was LSC for PZT films and Ti/Pt for PSKNN films. Table 3 summarizes the ferroelectric properties of the PZT and PSKNN thin films. The dielectric constant for PZT deposited on SBN is over

1800, and polarization is 33-36 $\mu C/cm^2$. In the case of PSKNN films, preliminary results show a dielectric constant of 1000 and a remanent polarization of 23 $\mu C/cm^2$. Since the polarization values in dense PSKNN ceramics near the MPB are typically near 40 $\mu C/cm^2$, we expect the polarization values >40 $\mu C/cm^2$ in these films. We are accurately measuring the lattice constants for the PSKNN films to determine the relationship between lattice constant and polarization.

Figure 7(a) shows the P-E hysteresis of a PZT thin films on MgO/LSC measured at 23 °C at a frequency of 25 Hz after 5.5 x 10^7 cycles. The maximum applied field is ± 62 kV/cm, with a film coercive field E_c = 29 kV/cm. Above 80 kV/cm, the curve begins to distort in a manner suggesting nonlinear space charge limited current injection. The remnant polarization at zero bias was measured at 19 $\mu C/cm^2$. Figure 7(b) shows the hysteresis loop for a PZT film on SBN:60/LSC after 1.1 x 10^9 cycles. P_r is 33-36 $\mu C/cm^2$ with only a slight increase in E_c to 36 kV/cm. This comparison clearly suggests that the crystallinity of PZT films on SBN substrate is much better, and further improvements in the characteristics are possible using SBN substrates for optical applications. Furthermore this value changes little with hysteresis cycles beyond 10^8, this is a reflection of the good lattice match with the LSC/SBN layer the absence of film defects which can cause substantial fatigue.

Table 3

Properties of PZT and PSKNN Thin Films Grown on SBN:60 Substrates

Property	PZT	PSKNN
Dielectric Constant (ϵ)	1830-1890	1000
Polarization ($\mu C/cm2$) at 23°C	33 - 36	> 23
Coersive Field, E_c (kV/cm)	27 - 35	< 20
Refractive Index	2.475 - 2.478	2.423 - 2.456
Phase Transition Temp. T_c (°C)	~ 355	~ 165

Using the relations $r_{33} = 2g_{33}P_3\epsilon_{33}\epsilon_0$ and $r_{51} = g_{44}P_3\epsilon_{11}\epsilon_0$, and our measured polarization and dielectric constant for these films, we estimated r_{51} ~ 600-800 x 10^{-12} m/V for PZT and r_{33} ~ 500-600 x 10^{-12} m/V for PSKNN. Although there is room for improvement in these films, particularly regarding film stoichiometry and quality in the case PSKNN, these materials can be grown successfully on SBN:60 and perovskite $LaAlO_3$ (or cubic $NdGaO_3$) substrates which provide a very good lattice match to the films. Further work now remains to improve the film growth processes to obtain films with reduced optical defects and optical losses so that they may be successfully used in a variety of optical applications.
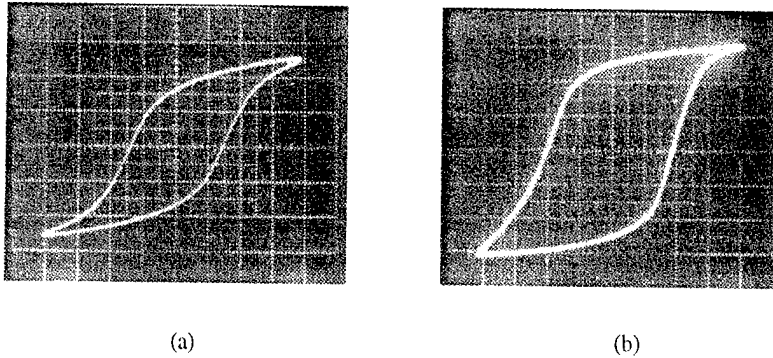
(a)   (b)

Figure 7 - Polarization vs electric field for a PZT film deposited on SBN:60 &MgO
(a) $P_r = 36.5$ $\mu C/cm^2$ for PZT on SBN:60 and (b) $P_r = 19$ $\mu C/cm^2$ for PZT on MgO.

The figure-of-merit (FOM) for various ferroelectric materials has been summarized in Fig. 8. At present, $LiNbO_3$ and $LiTaO_3$ are used predominately for optical applications, including guided-wave optics, frequency conversion, and photorefractive applications. Although $LiNbO_3$ and $LiTaO_3$ exhibit superior performance in optical wave guides, these materials require high operating voltages. Recent work by Eknoyan et al [8-10] has shown that using high electro-optic coefficient SBN:60 ($r_{33} = 420 \times 10^{-12}$ m/V) and BSTN ($r_{33} \geq 250 \times 10^{-12}$ m/V), the operating voltages are almost an order of magnitude lower in these crystals as compared to $LiNbO_3$. Because of such low operating voltages, they were available to fabricate compact waveguides. The ferroelectric and optical measurements on ceramic and crystal samples of MPB materials show substantial enhancement in these properties, which will provide a decrease in operating voltages. As the compositional control and optical quality in these films continue to improve, e.g. using our SBN:60 substrates, the MPB thin films hold great promise for future generations of optical applications.
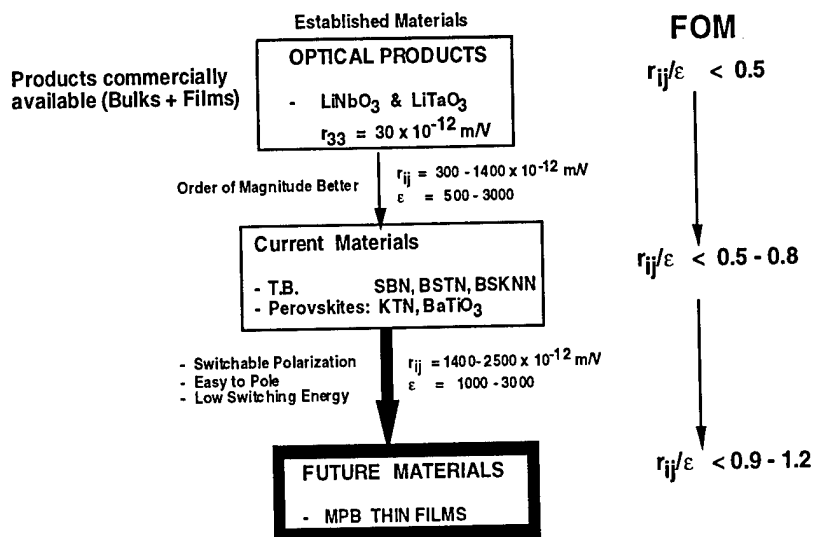
Established Materials

Products commercially available (Bulks + Films)

OPTICAL PRODUCTS

- $LiNbO_3$ & $LiTaO_3$
  $r_{33} = 30 \times 10^{-12}$ m/V

FOM

$r_{ij}/\varepsilon < 0.5$

Order of Magnitude Better

$r_{ij} = 300 - 1400 \times 10^{-12}$ m/V
$\varepsilon = 500 - 3000$

Current Materials

- T.B.   SBN, BSTN, BSKNN
- Perovskites: KTN, $BaTiO_3$

$r_{ij}/\varepsilon < 0.5 - 0.8$

- Switchable Polarization
- Easy to Pole
- Low Switching Energy

$r_{ij} = 1400 - 2500 \times 10^{-12}$ m/V
$\varepsilon = 1000 - 3000$

FUTURE MATERIALS

- MPB THIN FILMS

$r_{ij}/\varepsilon < 0.9 - 1.2$

Figure 8 - Summarizes the optical figure-of-merit for various ferroelectric materials.

REFERENCES

1. H. F. Taylor, Proc. IEEE **75**, 1524 (1987).
2. L. Thylen, J. Lightwave Technology **6**, 847 (1988).
3. R. V. Schmidt and I. P. Kaminow, Appl. Phys. Lett. **25**, 458 (1974)
4. M. L. Sah, Appl. Phys. Lett. **26**, 652 (1975).
5. J. L. Jackel, Appl. Opt. **19**, 1966 (1980).
6. D. W. Yoon and O. Eknoyan, J. Lightwave Technology **6**, 877 (1988).
7. O. Eknoyan, C. H. Bulmer, H. F. Taylor, W. K. Burns, A. S. Greenblatt, L. A. Beach and R. R. Neurgaonkar, Appl. Phys. Lett. **48**, 13 (1986).
8. J. M. Marx, Z. Tang, O. Eknoyan, H. F. Taylor and R. R. Neurgaonkar, Appl. Phys. Lett. **66**, 274 (1995).

9. O. Eknoyan, V. P. Swanson, J. D. Quinn and R. R. Neurgaonkar, Appl. Phys. Lett. **59**, 28 (1991).

10. E. Eknoyan, H. F. Taylor and R. R. Neurgaonkar, Submitted to Appl. Phys. Lett. (1995).

11. Y. Shimizu, K. R. Udayakumar and L. E. Cross, J. Am. Ceram. Soc. **74**, 3023 (1991).

12. R. R. Neurgaonkar, I.S. Santha, J.R. Oliver, J.G. Nelson, J.T. Cheung and P.E.D. Morgan, Mat. Res. Bull. **28**, 719 (1993).

13. J. T. Cheung, P. E. D. Morgan and R. R. Neurgaonkar, Private Communication.

14. B. Jaffe, W. R. Cook and H. Jaffe, " Piezo Ceramics", Academic Press (1971).

15. T. R. Shrout, H. Chen and L. E. Cross, Ferroelectrics **56**, 45 (1983).

16. T. R. Shrout, L. E. Cross and H. A. Dukin, Ferroelectrics Lett. **44**, 325 (1983).

17. J. R. Oliver, R. R. Neurgaonkar and L. E. Cross, J. Appl. Phys. **64**, 37 (1988).

18. R. R. Neurgaonkar, J. R. Oliver, W. K. Cory, L. E. Cross and D. Viehland, Ferroelectrics **160**, 265 (1994).

19. J. R. Oliver, R. R. Neurgaonkar and L. E. Cross, Am. Ceram. Soc. **72**, 202 (1989).

GRAIN ORIENTED FERROELECTRIC PZT THIN FILMS ON
LATTICE-MATCHED SUBSTRATES

R. R. Neurgaonkar, I. S. Santha, J. R. Oliver, J. G. Nelson,
J. T. Cheung and P.E.D. Morgan
Rockwell International Science Center
Thousand Oaks, CA 91360

and

K. R. Udayakumar
Pennsylvania State University
University Park, PA 16802

ABSTRACT

The sol-gel technique has been used to produce highly grain-oriented perovskite PZT thin films on lattice-matched SBN:60, $SrTiO_3$ and MgO substrates. These films were deposited on both $La_{0.5}Sr_{0.5}CoO_3$ (LSC) laser ablated-coated and uncoated substrates and annealed in the range of 630-675°C in an air or oxygen atmosphere. In all cases the PZT thin films were highly crystalline and oriented, with dielectric constants higher than 1100. The measured remanent polarization in these films exceeded 18 $\mu coul/cm^2$ indicating the potential for strong electro-optic and piezoelectric effects.

MATERIALS INDEX: thin films, ferroelectric materials, sol-gels

Introduction

Ferroelectric thin films that are highly grain-oriented are crucial elements in various electro-optic and photorefractive device concepts such as optical modulators and holographic switches. Fabrication of such films has proven difficult, particularly when precise compositional control is needed. We have grown various tungsten bronze and

perovskite ferroelectric films on SBN substrates using liquid phase epitaxy (LPE), sputtering and sol-gel techniques (1-8). In the first two cases film composition is hard to control, while in the sol-gel process, obtaining grain-orientation is difficult.

In this paper, we report the successful growth of highly grain-oriented PZT thin films on various lattice-matched substrates (SBN:60, $SrTiO_3$ and MgO) by the sol-gel technique. We were encouraged to try this technique by the success of Hirano et al. (9) in the growth of grain-oriented $LiNbO_3$ films on sapphire (Al_2O_3). While single crystal PLZT films have been produced on lattice-matched $SrTiO_3$ by the rf sputtering technique (10), this is the first demonstration of sol-gel growth to produce highly crystalline ferroelectric PZT films on tungsten bronze SBN, $SrTiO_3$ and MgO substrates. In addition interesting results were obtained when using an electrical conducting buffer layer of $La_{0.5}Sr_{0.5}CoO_3$ (LSC). Highly electrically conducting perovskites have been known for many years (11), with LSC particularly known to exhibit outstanding high electrical conductivity (12, 13) and lattice parameters (14) suitable for matching to many ferroelectric (and other perovskites) materials. Thus epitaxial metallic electrode/insulating interfaces can be achieved with minimal stress which then may be anticipated to demonstrate very good fatigue properties.

Experimental Procedure

1. Preparation of Stock Solution

The procedure followed for preparation of sol-gel solutions has been outlined in detail by Udayakumar et al. (15,16). Lead acetate trihydrate was dissolved in heated 2-methoxyethanol at a 1:26 molar ratio in a three-neck reaction flask. The solution was then heated to above 100°C and maintained at the same temperature for 1-2 hours to remove the water of hydration. The dehydrated solution was cooled to room temperature before the required amount of titanium iso-propoxide and Zirconium-n-propoxide were added sequentially under a dry argon atmosphere. The solution was then refluxed for several hours to promote complexation. Thereupon, the solution was heated until the temperature of the condensing vapor reached that of pure 2-methoxyethanol. The final concentration of the solution was adjusted to 1 M by either the removal or addition of 2-methoxyethanol. The 1M complex alkoxide solution was stored in a dry box.

As discussed by Shimuzi et al. (15), a thin-film precursor solution was prepared by combining equal volumes of the stock solution and 2-methoxyethanol. Hydrolysis was realized from the moisture in the ambient. Thin films fabricated from solutions prepared by a similar procedure delineated above have reproducibly shown excellent electrical characteristics (17).

2. Thin Film Growth

The substrate structure employed in this study consisted of 500Å Ti / 1000Å Pt and $La_{0.5}Sr_{0.5}CoO_3$ (LSC) as a buffer layer applied by laser ablation (8,18) on lattice-matched SBN:60, MgO and $SrTiO_3$ substrates. Thin films were fabricated on the substrate by spin coating at 3000-5000 rpm for 25 seconds. Following the procedure of Dey and Zuleeg (19), the films were pyrolyzed in air above 200°C, and the cycle was repeated until the desired thickness was obtained. In the present work, film thicknesses were in the range of 0.5 to 2.0 μm to establish the ferroelectric and structural properties.

The film-coated samples were annealed at elevated temperatures in air or oxygen for a period of 2 to 3 hours. In the annealing process, the films were first held at 400°C for 30 minutes to ensure the complete pyrolysis of the organic with a heating rate of 10°C/min., and 5°C/min thereupon to the final annealing temperature (630-675°C). Since SBN substrates are ferroelectric at room temperature, films grown on SBN were cooled slowly through the phase transition temperature (78°C) to avoid cracking.

3. Thin Film Characterization

The phase purity and grain-orientation of the films were characterized by various x-ray diffraction techniques. The chemical composition of the films was determined by scanning electron microscopy. For ferroelectric measurements, platinum surface electrodes were used. The relative dielectric constant and dielectric loss tangent of the films were measured as a function of temperature and frequency using a multifrequency LCR meter (4274A, Hewlett Packard Co.). The polarization- field (P-E) hysteresis loop and fatigue were measured using a modified Sawyer-Tower circuit at 23°C .

Results and Discussion

Table 1 summarizes growth conditions for the PZT films and the results of each growth in terms of film thickness and degree of orientation. The most extensive set of growth experiments were carried out on SBN substrates. These included two different orientations with no buffer layer and conducting LSC buffer layer. The conducting buffer layer allows direct measurements of the ferroelectric properties of the PZT films.

TABLE 1
Growth Conditions for PZT Films

Substrate	Annealing Temp (°C)	Thickness (μm)	Film Orientation	Unit Cell (Å)
SBN Substrate				
(001) No Coating	640-675	0.5 to 1.5	(100) oriented	4.015
(001) LSC-Coating	620-640	0.5 to 1.0	(100) oriented	4.021
(100) No Coating	640-675	0.5 to 1.0	polycrystalline	---
SrTiO₃ Substrate				
(100) No Coating	620-635	0.5 to 1.0	(100) oriented	3.992
(100) LSC Coating	620-635	0.5 to 1.2	(100) oriented	3.995
MgO Substrate				
(100) No Coating	640-650	0.5 to 1.0	partially oriented	4.081
(100) LSC Coating	640-650	0.5 to 1.0	(100) oriented	4.081

As shown by the x-ray diffraction patterns in Figure 1, the PZT films deposited on (001) SBN:60 substrates are highly oriented along the (100) direction of the perovskite structure because of the close lattice match between (100) PZT and (001) SBN:60. This is the first time the sol-gel process has been successfully used to grow highly grain-oriented PZT films on SBN. Since the refractive index difference between PZT

and SBN:60 is large ($\Delta n \sim 0.218$), this structure could have significant impact on photorefractive and electro-optic applications. We are currently adjusting the film composition to improve the lattice match with SBN:60, which will lead to lower strain and lower defect oriented films. In contrast, PZT films grown on (100)-oriented SBN:60 substrates are typically lattice-mismatched and therefore the films are polycrystalline with no preferred orientation.

Also shown in Figure 1 is the diffraction pattern for PZT grown on SBN/LSC. The LSC buffer layer grows as a highly oriented cubic perovskite on SBN:60 with a lattice constant slightly lower than the c-axis value for SBN. For this reason, the subsequent PZT layer also achieves good grain orientation.

Figure 2 shows the x-ray diffraction patterns for grain-oriented PZT films on LSC coated $SrTiO_3$ and MgO. Since the film, substrate and buffer layers are all perovskite, we expected that the crystallinity of the PZT films on $SrTiO_3$/LSC should be good. It has been reported that single crystal PZT films have been grown by rf sputtering on (100)-oriented $SrTiO_3$ substrates for optical applications (10), but this is the first instance of sol-gel growth of such films. Efforts are under way to study the film quality for optical applications using (110) and (111)-oriented $SrTiO_3$ substrates.

PZT films deposited on (100)-oriented MgO substrates also indicated high grain orientation, as shown by the x-ray diffraction pattern in Figure 3. The unit cell dimension established for the PZT film (c = 4.081Å), using the d-values for the oriented pattern, is significantly larger than the unit cell dimension obtained for PZT films on SBN or $SrTiO_3$ substrates (Table 1). We believe that the films deposited on MgO are oriented along the (001) direction because the unit cell dimensions of PZT along the c-axis are larger (> 4.07Å) and are close to that of MgO (~ 4.21Å). Further work is in progress to support this result.

Electrical measurements were carried out using Pt contact pads of either 0.00485 cm^2 or 0.0182 cm^2 area sputtered onto the film surface. Figure 3 shows the temperature dependence of the weak-field dielectric constant at 100 kHz for a PZT film on MgO/LSC. The ferroelectric phase transition, indicated by the dielectric maximum, is at 396°C, somewhat higher than expected for a near-morphotropic PZT composition. The dielectric properties at lower frequencies are similar to that shown in Figure 3 except for the appearance of excess boundary layer capacitance above 350°C due to the large conductivity in this region. Above 400°C, the conductivity is nearly frequency-independent with an activation energy of 1.1 eV, a value considerably shallower than the 1.4 - 1.5 eV we have typically observed in good quality PZT ceramics. This suggests that the film stoichiometry is not yet as good as it could be.

Figure 4(a) shows the P-E hysteresis of the same PZT thin film measured at 23°C at a frequency of 25 Hz. The maximum applied field is ± 62 kV/cm, with a film coercive field E_c = 27 kV/cm. Above 80 kV/cm, the curve begins to distort in a manner suggesting non-linear space charge limited current injection consistent with the electronic Fermi level being far removed from a mid-gap position. The remanent polarization at zero bias was measured at 36 - 39 μcoulombs/cm^2, but because of the aforementioned space charge limited currents, these values may overestimate the true remanent polarization by up to 30%. Figure 4(b) shows the hysteresis loop for a PZT film on MgO/LSC after 5.5 x 10^7 cycles, with the vertical (polarization) scale expanded by a factor of two for clarity. P_r has reduced to 19.0 μcoulombs/cm^2 with only a slight
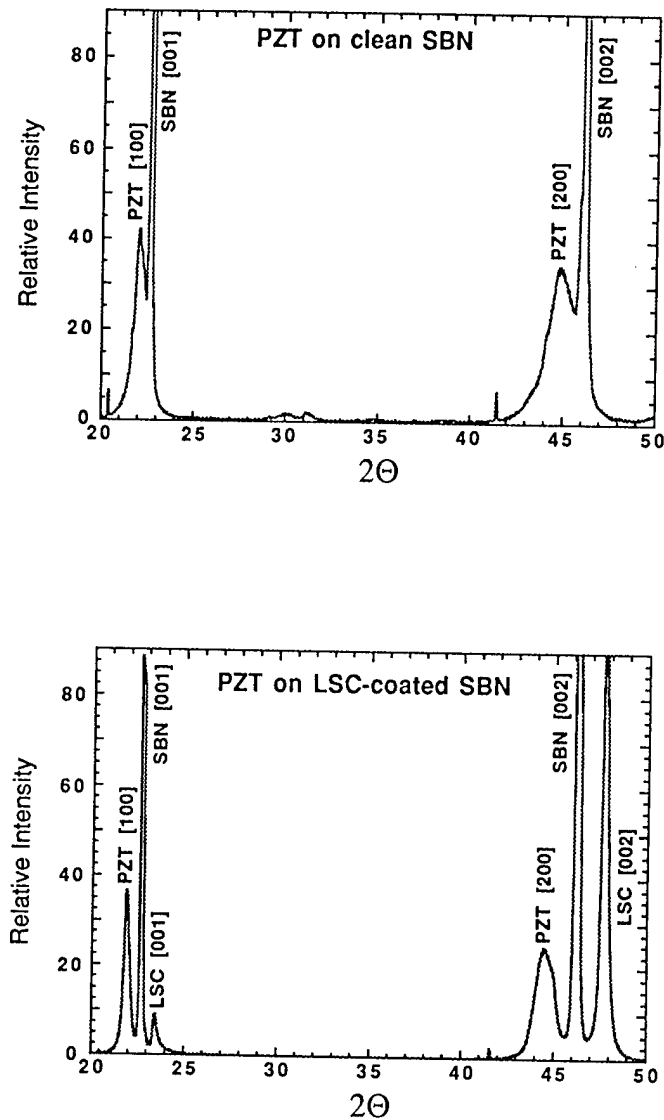
Figure 1 - X-ray diffraction pattern of PZT films on SBN substrates.

increase in E_c to 29 kV/cm. The fatigue behavior of the remanent polarization with repeated hysteresis cycles is shown in Figure 5, where it is seen that P_r remains essentially constant above 6×10^6 cycles with no evidence of any further fatigue up to 2.6×10^8 cycles. In light of the discussion above, it is uncertain how much of this fatigue behavior may be attributed to an actual decline of P_r. Nevertheless, the limiting value of 18.5 μcoulombs/cm^2, which remains essentially constant even for field maxima above 100 kV/cm, is extremely good.

Figure 2 - X-ray diffraction patterns for PZT films on (a) SrTiO$_3$ and (b) MgO substrates with intervening LSC layer.

Table 2 summarizes the room-temperature properties of the sol-gel PZT thin films grown on MgO, SBN:60 and SrTiO$_3$ substrates with intervening LSC contact layers. PZT films grown on the latter two substrates showed superior high-field behavior with essentially no evidence of space charge current injection or film breakdown for electric fields up to 130 kV/cm.
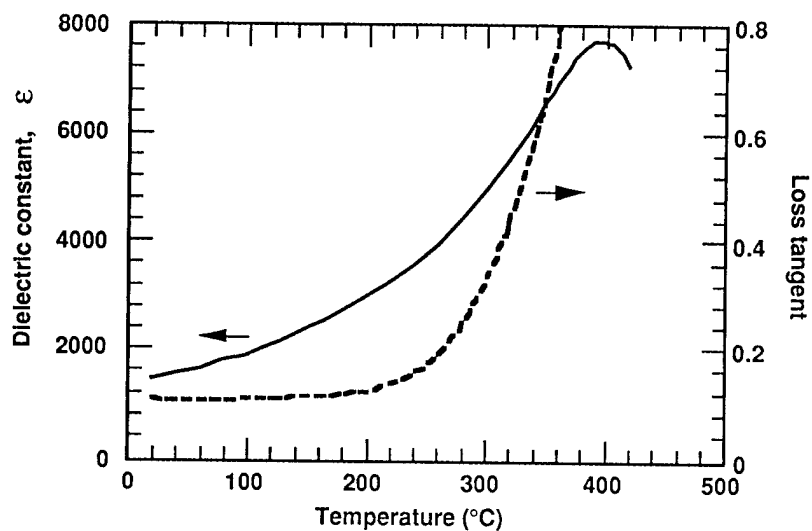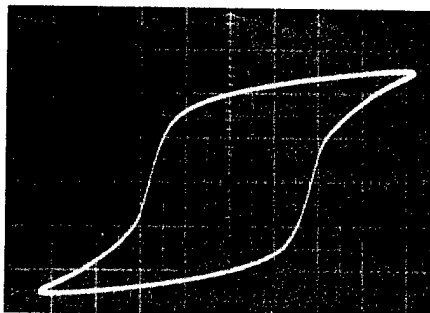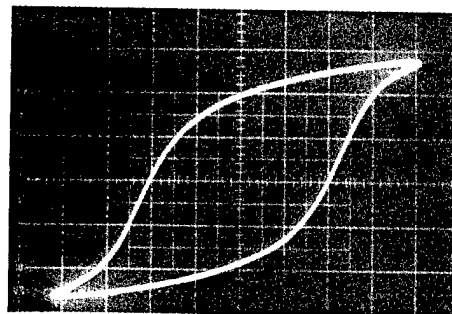
Figure 3 - Temperature dependence of the dielectric constant and Tan δ
at 100 kHz for a PZT Film on MgO/LSC

(a) After 500 cycles. f = 25 Hz,
P_r = 36.5 μcoul/cm^2.

(b) After 5.5 x10^7 cycles.
P_r = 19 μcoul/cm^2. Vertical scale
expanded 2X.

Figure 4 - Polarization vs electric field for a PZT film deposited on MgO.

TABLE 2
Properties of PZT Films Grown on SBN, SrTiO$_3$ and MgO Substrates

Substrate	ε	P_3 (μcoul/cm^2)		E_c (kV/cm)
		as measured	after 2x10^8 cycles	
MgO	1390	36.5	19.0	27
SBN:60	1830	23.0	----	32
SrTiO$_3$	1100	19.0	----	38

$P_r(0) = 36.5$ μcoul/cm^2

at 2.6x10^8 cycles :

$P_r/P_r(0) = 0.507$

$Pr = 18.5$ μcoul/cm^2

Figure 5 - Electrical fatigue for a PZT film on MgO/LSC.

Conclusions

We have presented our preliminary work on the growth of highly grain-oriented PZT films using the sol-gel technique. These films show high remanent polarization and high dielectric constants, indicating that the electro-optic and piezoelectric properties should be proportionately large. These properties can be increased further by adjusting the film composition and stoichiometry . The successful development of these films will open up a variety of optical applications using the electro-optic effect (modulators and waveguides) and the photorefractive effect (switches, image processing, pattern recognition and neural network).

Acknowledgments

References

1. R. R. Neurgaonkar, M. H. Kalisher, E. J. Staples and T. C. Lim, Appl. Phys. Lett. 35 (8), 606 (1979).
2. R. R. Neurgaonkar, T. C. Lim, E. J. Staples and L. E. Cross, Ferroelectrics 27, 62 (1980).
3. R. R. Neurgaonkar and E. J. Staples, J. Cryst. Growth 27, 352 (1981).
4. R. R. Neurgaonkar and E. T. Wu, Mat. Res. Bull. 22 (8), 1095 (1986).
5. R. R. Neurgaonkar, J. R. Oliver and L. E. Cross, Mat. Lett. 6 (5-6), 152 (1988).
6. R. R. Neurgaonkar, I. Santha, J. R. Oliver, E. T. Wu and L. E. Cross, J. Mat. Science 25, 2053 (1990).
7. R. R. Neurgaonkar, I. S. Santha and J. R. Oliver, submitted to Mat. Res. Bull.
8. J. T. Cheung, P. E. D. Morgan and R. R. Neurgaonkar, private communication.
9. S. Hirano, T. Yogo, K. Kikuta, K. Kals, W. Sakamoto and S. Ogasahara, Ceram. Transaction 25, 19 (1991).
10. Y. Higuma, K. Tanaka, T. Nakagawa, T. Kariya and Y. Hamakawa, (Jap) J. Appl. Phys. 16 (9), 1707 (1977).
11. P. E. D. Morgan, Proc. Workshop on High Temperature Solid Oxide Fuel Cells, H. S. Isaacs, S. Srinivasan and I. L. Harry, Eds., BNL 50765, 54 (1977).
12. G. H. Jonker and J. H. Van Santen, Physica 19, 120 (1953).
13. P. E. D. Morgan, J. Am. Ceram. Soc. 58, 349 (1975).
14. P. M. Raccah and J. Goodenough, J. Appl. Phys. 39, 1209 (1968).
15. Y. Shimizu, K. R. Udayakumar and L. E. Cross, J. Am. Ceram. Soc. 74 (12), 3023 (1991).
16. K. R. Udayakumar, J. Chen, S. B. Krupanidhi and L. E. Cross, Proc. of 7th IEEE, ISAF, 741 (1990).
17. K.R. Udayakumar, S.F. Bart, A.F. Flint, J. Chen, L. Tavrow, L.E. Cross, R. Brook and D.J. Ehrlich, Proc. 4th IEEE Workshop on Microelectro Mechanical Systems, 109 (1991).
18. P. E. D. Morgan, 14th University Conf., "Processing of Crystalline Ceramics," Materials Science Research 11, 67, Eds, H. Pamour III, R. F. Davis, T. M. Hare, Plenum Press (1978).
19. S. K. Dey and R. Zuleeg, Ferroelectrics 108, 37 (1990).

Appendix 7.3

Ferroelectric PZT Thin Films On Si and SBN Substrates

Ferroelectric PZT thin films on Si and SBN substrates

Ratnakar R. Neurgaonkar, Jeffrey G. Nelson, Joey Lin, and James Cheng

Rockwell International Science Center
1049 Camino Dos Rios
Thousand Oaks, CA 91360

ABSTRACT

The sol-gel technique has been used to produce perovskite PZT thin films on lattice-matched SBN:60 and LaAlO$_3$ substrates. These films were spin-coated and then annealed in the range of 500 - 700 °C in an oxygen atmosphere. Highly grain oriented films showed high polarization and the potential for a large electro-optic response. In all cases, the PZT thin films were highly crystalline, with dielectric constants > 1300. PZT films were also deposited on Pt-metallized Si using the same deposition technique in order to establish the effect of annealing conditions on the formation of pyrochlore phase.

Keywords: piezoelectric, thin films, PZT, sol-gel, lattice-matched substrates

1. INTRODUCTION

Piezoelectric thin films that are highly crystalline are crucial elements in various electro-optic, micro-opto-electro-mechanical and piezoelectric device concepts such as optical modulators, holographic switches and accelerometers. Fabrication of such films has proven difficult, particularly when precise compositional control is needed. We have grown various tungsten bronze and perovskite ferroelectric films on SBN substrates using liquid phase epitaxy (LPE), sputtering and sol-gel techniques.[1-6] In the first two cases film composition is hard to control, while in the sol-gel process, obtaining grain-orientation is difficult.

In this paper, we report the successful growth of highly grain-oriented PZT thin films on various lattice-matched substrates (SBN:60 and LaAlO$_3$) by the sol-gel technique. We were encouraged to try this technique by the success of Hirano et al.[7] in the growth of grain-oriented LiNbO$_3$ films on sapphire (Al$_2$O$_3$). While single crystal PLZT films have been produced on lattice-matched SrTiO$_3$ by

the rf sputtering technique,[8] it is important to establish the sol-gel growth as a means of producing highly crystalline ferroelectric PZT films on tungsten bronze SBN and LaAlO3 substrates.

In addition to lattice-matched substrates, Pt-metallized Si substrates were used in a series of experiments designed to establish the lowest annealing temperature at which pyrochlore-free PZT can be obtained. Certain applications such as temperature-sensitive devices and low melting point substrates could benefit greatly from the ability to deposit good quality PZT films.

2. EXPERIMENTAL PROCEDURE

2.1 Preparation of stock solution

The procedure followed for preparation of sol-gel solutions has been outlined in detail by Udaykumar et al.[9,10] Lead acetate trihydrate was dissolved in heated 2-methoxyethanol at a 1:26 molar ratio in a three-neck reaction flask. The solution was then heated to above 100 °C and maintained at the same temperature for 1-2 hours to remove the water of hydration. The dehydrated solution was cooled to room temperature before the required amount of titanium iso-propoxide and zirconium iso-propoxide was added sequentially under a dry argon atmosphere. The solution was then refluxed for several hours to promote complexation. Thereupon, the solution was heated until the temperature of the condensing vapor reached that of pure 2-methoxyethanol. The final concentration of the solution was adjusted to 1 M by either the removal or addition of 2-methoxyethanol. The 1M complex alkoxide solution was stored in a dry box.

As discussed by Shimuzi et al.,[9] a thin-film precursor solution was prepared by combining equal volumes of the stock solution and 2-methoxyethanol. In this work, we did not add water to the precursor solution, because the presence of even trace amounts of water resulted in high viscosity due to rapid gelation and was not suitable for the preparation of thin films by spin coating. Hydrolysis was realized from the moisture in the ambient.[11] Thin films fabricated from solutions prepared by a similar procedure delineated above have reproducibly shown excellent electrical characteristics.

2.2 Thin film growth

The substrate structures employed in this study consisted of either Pt-metallized Si or clean lattice-matched SBN:60 and LaAlO3 substrates. The metallization layers were deposited at ambient temperature without the need for any post-deposition annealing. The PZT thin films were fabricated on

the substrate by spin coating at 3000 rpm for 30 seconds. Following the procedure of Dey and Zuleeg,[12] the films were pyrolyzed in air above 300 °C, and the cycle was repeated until the desired thickness was obtained. Using profilometer measurements, it was determined that ~750 Å of PZT was deposited during each spin coating. In the present work, film thicknesses were in the range of 0.5 to 1.5 µm to establish the ferroelectric and structural properties.

The film-coated SBN:60 and LaAlO$_3$ substrates were annealed using rapid thermal processing (RTP) in oxygen for a period of 0.5 to 1 minute. In the annealing process, the films were first held at 400 °C for 30 seconds to ensure the complete pyrolysis of the organic with a heating rate of 100 °C/sec, and 250 °C/sec rate thereupon to the final annealing temperature (630-675 °C). Because of the rapid heating and relatively short time at temperature, the SBN substrates did not reach a sufficiently high temperature where cracking was a problem.

In the case of Pt-metallized substrates, RTP temperatures ranging from 500°C to 650°C were used. The temperature profile was similar to that used in the lattice-matched substrates, allowing a soak time of 30 seconds at 400°C before proceeding to the maximum temperature. Soak times ranging from 1 to 10 minutes were employed at the various maximum annealing temperatures to establish the role of time in the formation of perovskite PZT films. Since Si is much more robust than SBN:60 or LaAlO$_3$, cracking of the substrate or metallization layer was never observed in any of the annealing conditions used in these experiments.

2.3 Thin film characterization

The phase purity and grain-orientation of the films were characterized by various x-ray diffraction techniques. The chemical composition of the films was determined by scanning electron microscopy. For ferroelectric measurements, platinum surface electrodes were used. The relative dielectric constant and dielectric loss tangent of the films were measured as a function of temperature and frequency using a multifrequency LCR meter (4274A, Hewlett Packard Co.). The polarization- field (P-E) hysteresis loop and fatigue were measured using a modified Sawyer-Tower circuit at 23 °C.

3. RESULTS AND DISCUSSION

Table 1 summarizes the growth conditions for the PZT thin films and the results of each growth in terms of phase purity and degree of orientation. The most extensive set of growth experiments was performed on the metallized Si substrates while investigating the effect of annealing conditions on

perovskite phase formation. In the lattice-matched substrate experiments, LaAlO$_3$ was extensively used because we had already investigated the growth of PZT films on SBN:60 in some previous work.[13]

As shown by the x-ray diffraction patterns in Figure 1, the PZT films deposited on (001) SBN:60 substrates are highly oriented along the (100) direction of the perovskite structure because of the close lattice match between (100) PZT and (001) SBN:60. Since the refractive index difference between PZT and SBN:60 is large ($\Delta n \sim 0.218$), these films are potentially useful for photorefractive and guided-wave applications. Although the current films are suitable for these applications, we continue to improve the lattice match between the film and substrate by controlling the Zr:Ti ratio. This will reduce the strain and other defects in the highly oriented films. In contrast, PZT films grown on (100)-oriented SBN:60 substrates are typically lattice-mismatched and therefore the films are polycrystalline with no preferred orientation. Previously, PZT films grown on SBN using La$_{0.5}$Sr$_{0.5}$CoO$_3$ (LSC) electrodes[13] resulted in highly oriented, high polarization thin films.

TABLE 1
Growth Conditions for PZT Films

Substrate	Annealing Temp. (°C)	Annealing Time (minutes)	Film Orientation	Perovskite Phase (Percent)
SBN:60				
(001)	640 - 675	0.5 - 1.5	(100) oriented	100
(100)	640 - 675	0.5 - 1.0	polycrystalline	100
LaAlO$_3$				
(012)	630 - 675	0.5 - 1.2	(100) oriented	100
Pt/Ti/Si	500 - 675	0.5 - 1.05	polycrystalline	20 - 100

Figure 2 shows the x-ray diffraction patterns for grain-oriented PZT films on LaAlO$_3$. Even though the lattice mismatch ($\sim 4\%$) with LaAlO$_3$ with is not as low as that with SBN:60, the PZT films are highly oriented, showing only [100]-type reflections. The sharpness and the size of the PZT [100] and [200] peaks indicates that the films are highly crystallized while the pattern shows no indication of any pyrochlore phase. The ability to achieve grain orientation under these difficult conditions suggests that oriented films should be obtainable with a wide range of PZT compositions. Especially those with larger lattice constants and thus a smaller lattice mismatch with the LaAlO$_3$ substrate.
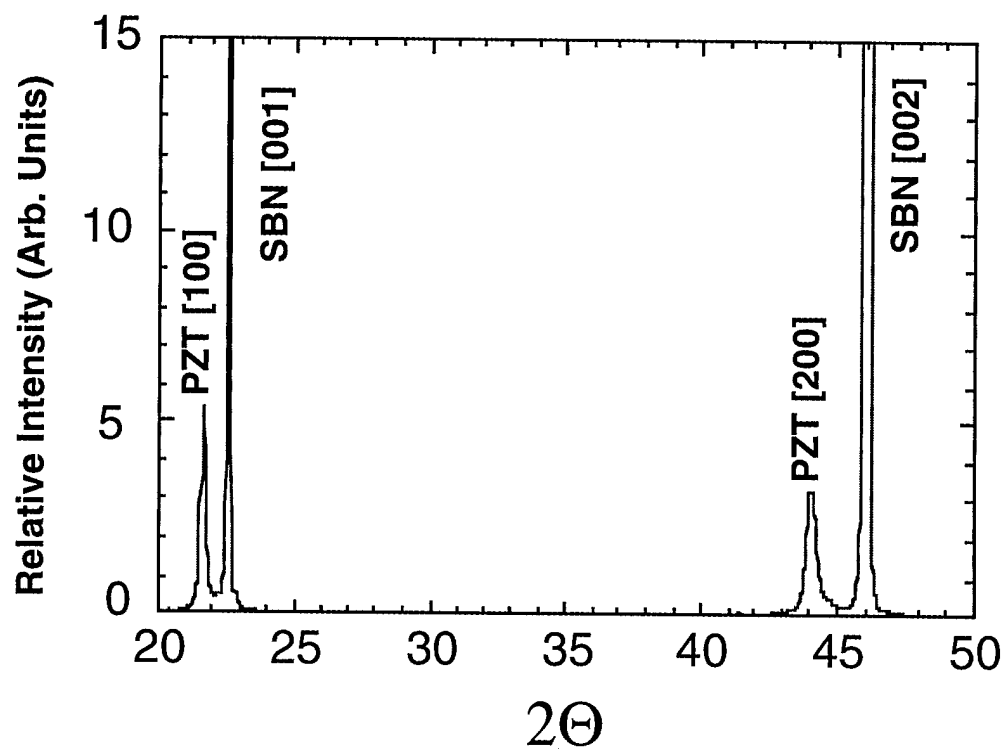
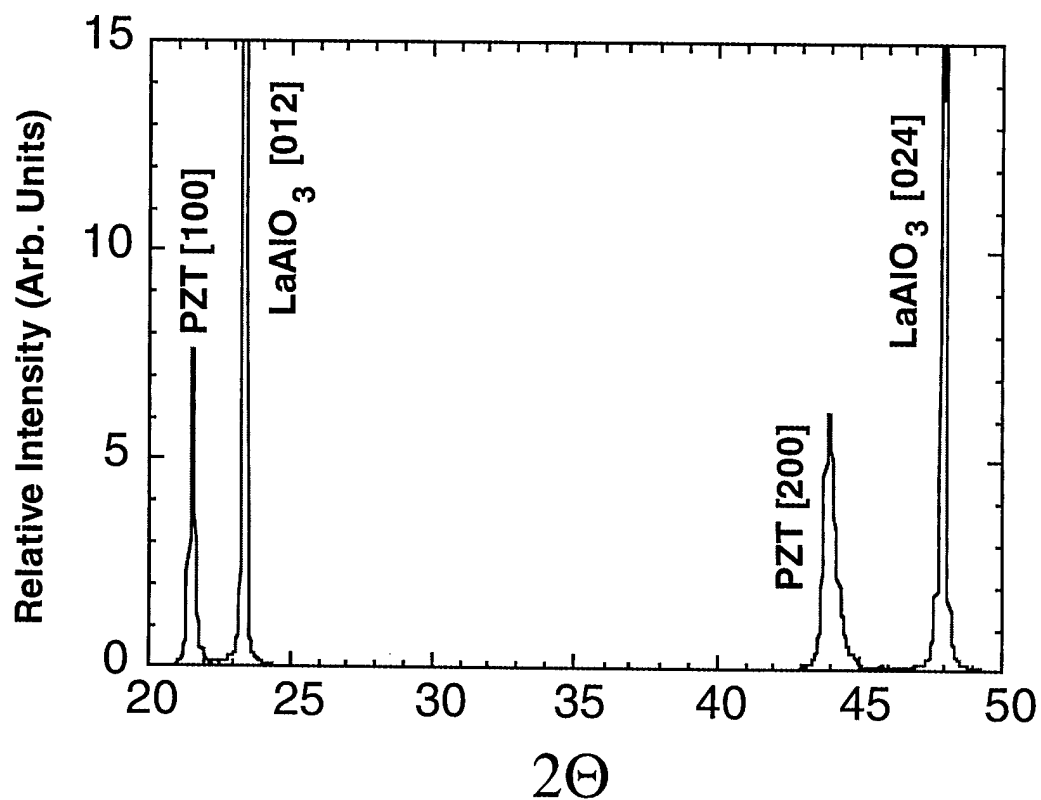Figure 1 - X-ray diffraction pattern of PZT thin film on SBN:60 substrate.

Figure 2 - X-ray diffraction pattern of PZT thin film on LaAlO$_3$ substrate.

In order to effectively measure the dielectric characteristics of these PZT thin films, electrodes must be deposited above and below the film. Deposition of a metallization layer on SBN:60 or LaAlO$_3$ substrates would disrupt the lattice match and destroy the high grain orientation of the PZT films. In our previous work,[13] we examined the use of La$_{0.5}$Sr$_{0.5}$CoO$_3$ (LSC) electrodes on various lattice-matched substrates for PZT deposition. Excellent grain orientation and high polarization (~30-35 μC/cm^2) was achieved using this system. However, standard metallization materials such as Ti/Pt and Cr/Au must be used with many MEMS applications in order to be compatible with traditional processing techniques. Consequently, we have explored the use of Pt-metallized Si substrates for PZT thin film growth

Figure 3 shows an x-ray diffraction pattern of a 0.95 μm thick PZT thin film grown on Pt-metallized Si, and as expected, the films are polycrystalline. These PZT thin films are well crystallized in the perovskite phase and show no indication of the presence of any pyrochlore phase. These films were annealed at 675 °C for 2 minutes.

The existence of pyrochlore phase was studied in these PZT films as a function of annealing temperature, and we found that the annealing conditions are crucial to eliminate the formation of this unwanted phase. Figure 4 shows a series of expanded x-ray diffraction patterns of 1.2 μm thick PZT thin films which were annealed at temperatures ranging from 500°C to 600°C. Two theta values of 20 to 35° were examined because they exhibit the perovskite PZT (100) and (110) reflections at 21.7° and 31°, respectively; in addition to the pyrochlore phase peak at 29.5°. This provides a convenient comparison of the relative amounts of the two phases. At 500°C annealing temperature, a significant amount of pyrochlore phase can be seen. However, as the temperature is increased the pyrochlore peak decreases until 600°C where no pyrochlore phase is detectable.

Time is also an important parameter in the overall annealing conditions. We expected that by extending the annealing to longer times than is usually used for RTP, we might further reduce the temperature needed to avoid the formation of pyrochlore phase. Annealing times ranging from 1 to 10 minutes over the temperatures previously described were examined. As seen in Figure 4, pyrochlore formation was observed at temperatures below 600°C for the maximum annealing time of 10 minutes. Figure 5 shows the x-ray diffraction pattern of 1.2 μm thick PZT films annealed at 600 °C for times ranging from 2 to 10 minutes. As expected, a significant amount of pyrochlore phase was observed at shorter annealing times. Only a trace of pyrochlore phase is seen at 8 minutes annealing, but 10 minutes is required to produce pure perovskite phase. Figure 6 summaries the results of the x-ray observations showing the amount of pyrochlore phase detected as a function of annealing time at 600°C.
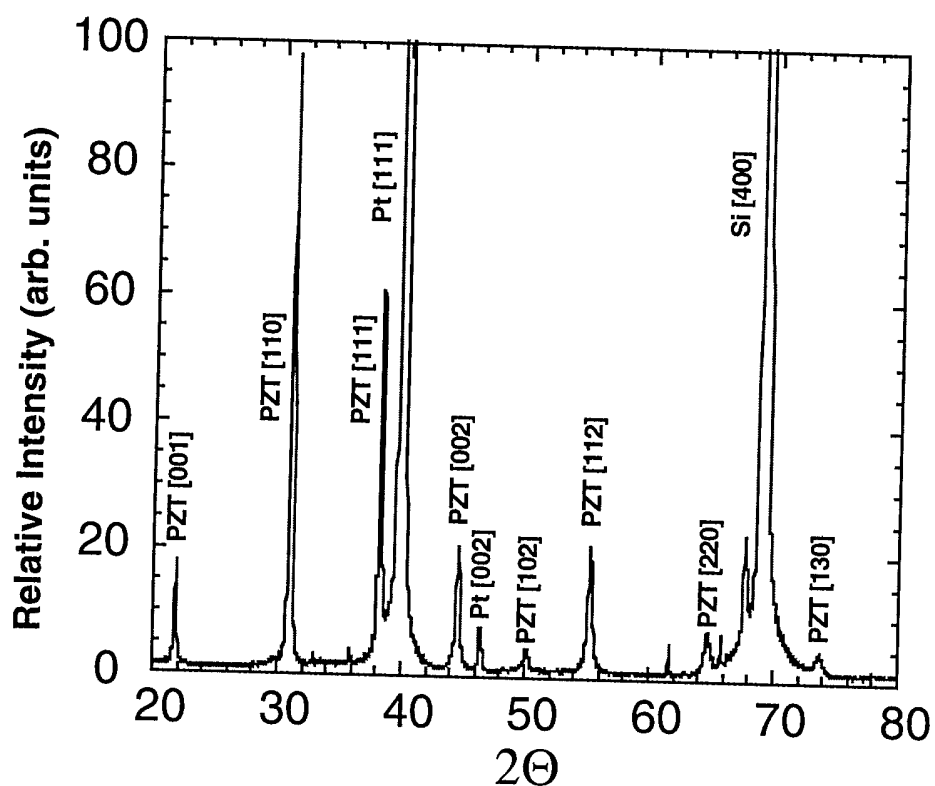
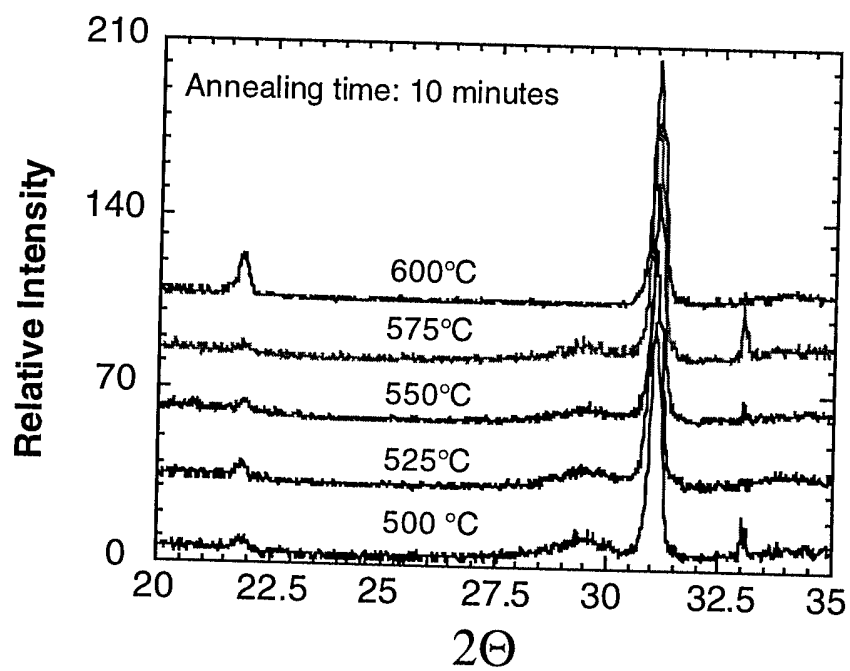Figure 3 - X-ray diffraction pattern of PZT thin film on metallized Si substrate.

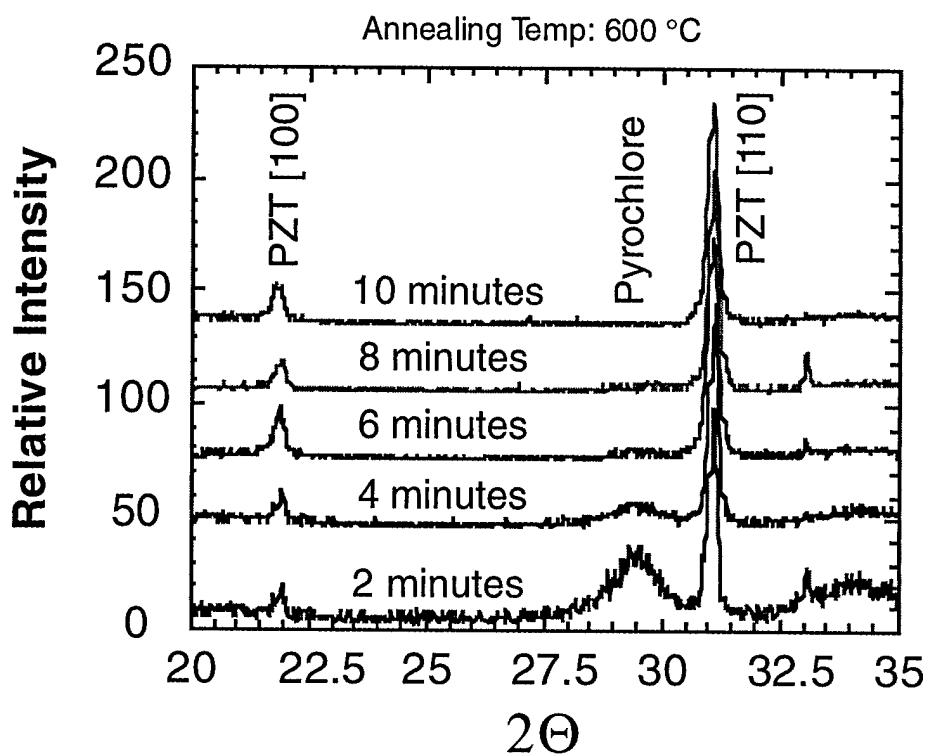Figure 4 - Effect of annealing temperature on the formation of pyrochlore phase in PZT films.

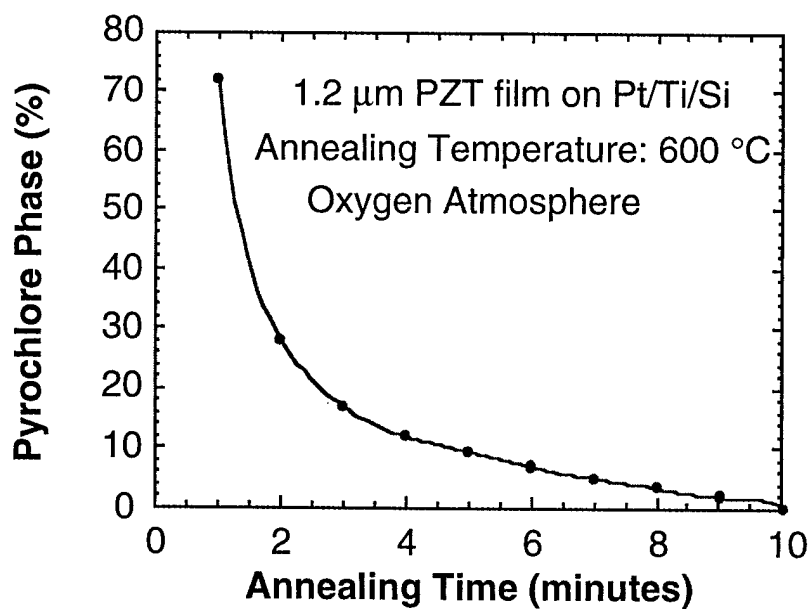Figure 5 - Effect of annealing time on the formation of pyrochlore phase in PZT films.

Figure 6 - Pyrochlore phase vs. annealing time for PZT film on metallized Si substrate.

Electrical measurements were carried out on PZT films grown on the metallized Si and lattice-matched substrates using Pt contact pads sputtered onto the film surface. The temperature dependence of the weak-field dielectric constant at 100 kHz as well as the P-E hysteresis was measured for the PZT films. Table 2 summarizes the dielectric and polarization measurements for PZT films grown on different substrates.

Table 2
Dielectric Properties of PZT Thin Films

Substrate/Electrode	CurieTemp. (°C)	ε (23°C)	P_S ($\mu C/cm^2$)	Reference
MgO/LSC	396	1380 - 1400	30 - 35	13
SBN:60/LSC	355	1830 - 1860	22 - 24	13
SBN:60/Pt	360	1900 - 2000	20 - 21	this work
Si/Pt	385	2000 - 2200	16 - 18	this work

The highest remanent polarization ($\sim$35 $\mu C/cm^2$) is seen on highly grain oriented PZT films such as those obtained with LSC electrodes. In these systems, the LSC electrode layer grows as a highly oriented cubic perovskite, with a lattice constant close to that of SBN:60. For this reason, the subsequent PZT film also achieves good grain orientation. The use of Pt as a metallization layer disrupts the lattice match and results in a polycrystalline PZT film with lower performance. However, work is still in progress on the SBN/Pt system, and improvements in the PZT performance is expected. These results also suggest that the polarization of PZT films deposited directly on SBN or LaAlO$_3$ should exceed 50 $\mu C/cm^2$ with a large electro-optic coefficient (r_{ij}). Many photorefractive and optical applications do not require the use of electrodes, therefore, PZT films deposited directly on lattice-matched substrates should result in superior performance in these devices.

In the case of Pt-,metallized Si, the ferroelectric phase transition, indicated by the dielectric maximum, is at 385°C, somewhat higher than expected for a near-morphotropic PZT composition. The room temperature dielectric constant of this film at 1 kHz was measured to be 2160. The dielectric properties at lower frequencies are similar to that seen at 100 kHz except for the appearance of excess boundary layer capacitance above 350°C due to the large conductivity in this region. Above 400 °C, the

conductivity is nearly frequency-independent with an activation energy of 1.25 eV, a value slightly shallower than the 1.4 - 1.5 eV we have typically observed in excellent quality PZT ceramics. This suggests that the film stoichiometry is not yet as good as it could be.

Figure 7 shows the P-E hysteresis of the same PZT thin film measured at 23°C at a frequency of 20 Hz. The maximum applied field is $\pm$ 78 kV/cm, with a film coercive field Ec = 15.5 kV/cm. The remanent polarization at zero bias was measured at 17.5 μcoulombs/cm^2, which is less than the values observed for grain oriented films. There are several possible explanations for this observed behavior. The measured dielectric constant of 2160 for these films is significantly higher than the value of ~1400 expected for near-morphotropic boundary compositions. This could be caused by disorder, defects or grain boundary conditions in the interfacial region between the PZT film and the metallization layer. Another possible explanation is compositional non-uniformity of the PZT film in this interfacial region. Either of these conditions can cause band bending at the PZT/Pt interface, resulting in the formation of an electric field in this region. This field can pin ferroelectric domains resulting in reduced domain motion and a significant reduction in the polarization. More experiments are planned to better establish the reasons for the reduced polarization in this system. The fabrication of grain oriented Pt metallization layers on Si substrates or the use of LSC electrodes could greatly improve the piezoelectric performance of these PZT thin films.
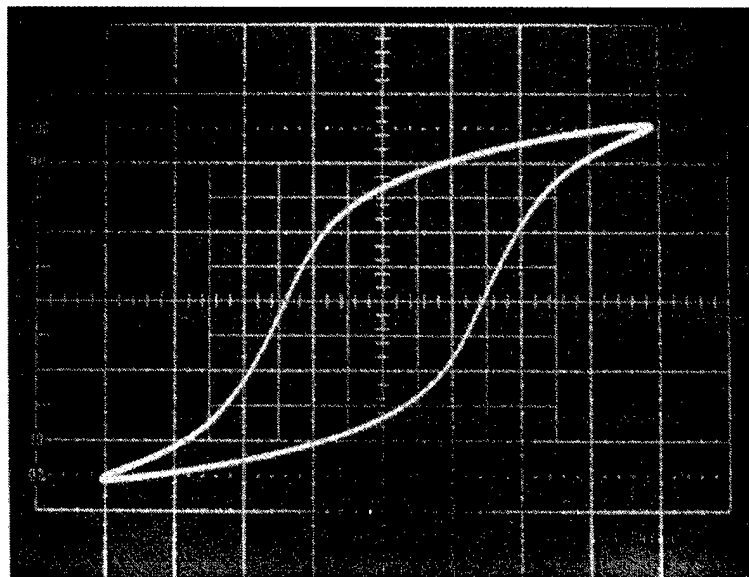

Figure 7 - P-E hysteresis loop of PZT film on Pt-metallized Si substrate.

4. CONCLUSIONS

We have presented the results of the growth of PZT thin films on Si and lattice-matched SBN:60 and LaAlO3 substrates using the sol gel technique. Using Pt-metallized substrates, lower temperature annealing conditions were established, which could be used with temperature sensitive devices and substrates. On lattice-matched substrates, these films show a high degree of grain orientation which results in good remanent polarization and high dielectric constants, indicating that the electro-optic and piezoelectric properties should be proportionately large. PZT films deposited directly on these substrates, without the need for electrodes, should result in excellent photorefractive and optical devices. The successful development of these films will open up a variety of other optical applications using the electro-optic effect (modulators and waveguides) and the piezoelectric effect (electronic memory).

5. ACKNOWLEDGMENTS

6. REFERENCES

1. R. R. Neurgaonkar, M. H. Kalisher, E. J. Staples and T. C. Lim, Appl. Phys. Lett. 35 (8), 606 (1979).
2. R. R. Neurgaonkar, T. C. Lim, E. J. Staples and L. E. Cross, Ferroelectrics 27, 62 (1980).
3. R. R. Neurgaonkar and E. J. Staples, J. Cryst. Growth 27, 352 (1981).
4. R. R. Neurgaonkar and E. T. Wu, Mat. Res. Bull. 22 (8), 1095 (1986).
5. R. R. Neurgaonkar, J. R. Oliver and L. E. Cross, Mat. Lett. 6 (5-6), 152 (1988).
6. R. R. Neurgaonkar, I. Santha, J. R. Oliver, E. T. Wu and L. E. Cross, J. Mat. Science 25, 2053 (1990).
7. S. Hirano, T. Yogo, K. Kikuta, K. Kals, W. Sakamoto and S. Ogasahara, Ceram. Transaction 25, 19 (1991).
8. Y. Higuma, K. Tanaka, T. Nakagawa, T. Kariya and Y. Hamakawa, (Jap) J. Appl. Phys. 16 (9), 1707 (1977).
9. Y. Shimizu, K. R. Udaykumar And L. E. Cross, J. Am. Ceram. Soc. 74 (12), 3023 (1991).
10. K. R. Udaykumar, J. Chen, S. B. Krupanidhi and L. E. Cross, Proc. of 7th IEEE, ISAF , 741 (1990).

11. G. A. Rossetti, T. Nishimura and L. E. Cross, J. Appl. Phys. 70 (3), 1630 (1991).
12. S. K. Dey and R. Zuleeg, Ferroelectrics 108, 37 (1990).
13. R.R. Neurgaonkar, I.S. Santha, J.R. Oliver, J.G. Nelson, J.T. Cheung, P.E.D. Morgan, and K.R. Udayakamar, Mat. Res. Bull. 28, 719 (1993).

Appendix 7.4

Monolithic Integration of a Silicon Driver Circuit onto a Lead PLZT Substrate for SLM Modulator Fabrication

Monolithic integration of a silicon driver circuit onto a lead lanthanum zirconate titanate substrate for smart spatial light modulator fabrication

M. S. Jin, J. H. Wang, V. Ozguz, and S. H. Lee

The monolithic integration of N-channel metal-oxide-semiconductor (NMOS) driver circuits in silicon thin films onto a lead lanthanum zirconate titanate (PLZT) substrate is reported. Two integration methods are compared. Both methods result in NMOS transistors that exhibit electrical properties that are close to those of transistors fabricated in bulk silicon. The characteristics of PLZT modulators driven by thin-film transistors are also similar to those of bulk PLZT modulators. These techniques promise new spatial light modulators of high complexity and performance that good-quality silicon and bulk PLZT can offer.

1. Introduction

The realization of smart spatial light modulators (S-SLM's) by the combination of electronic processing materials (e.g., Si and GaAs) and light modulation materials (e.g., ferroelectric ceramics or liquid crystals and III-V semiconductors) is essential for many tasks associated with the development of optoelectronic and optical computing. Recently, the possibility of fabricating sophisticated S-SLM's based on ferroelectric liquid-crystal and Si circuits has been demonstrated, but the operating speeds of these S-SLM's are relatively slow.[1–3] Exceptionally high modulation speed multiple-quantum-well-based S-SLM's, such as a field-effect transistor self-electro-optic-effect device (FET-SEED), have also been demonstrated, although the inherent absorption limits the light throughput and may cause a heat dissipation problem.[4] To find a better compromise between speed and light throughput, we have been studying S-SLM's that combine the mature Si electronic technology and lead lanthanum zirconate titanate (PLZT) (a transparent, ferroelectric ceramic) modulators. Their operating speeds are expected to be between those of the Si ferroelectric liquid-crystal and the

FET-SEED devices; the PLZT modulators do not absorb light.

In the past, other approaches for combining Si with PLZT have been studied.[5,6] However, in the approach in which a PLZT film is deposited on the windows of Si on sapphire, the light modulator is not effective because the maximum PLZT film thickness obtainable through deposition is far too thin. In the approach in which amorphous Si is deposited on bulk PLZT and then recrystallized, the quality of recrystallized Si is not high enough to implement large numbers of transistors and efficient light detectors.[7] In the flip-chip bonding approach, in which bulk quality Si is combined with bulk PLZT, there is a voltage compatibility problem that causes difficulties for inclusion of the modulator driver circuit (requiring 20–50 V) in the Si wafer that contains the logic circuits (operating at 5 V).

To overcome these limitations, we studied methods to bond Si-based driver circuits directly onto the bulk PLZT substrate. Sophisticated logic circuits would still be implemented in the bulk, foundry-processed Si wafers with excellent lifetime and minimum defect densities; this wafer will be flip-chip bonded to the Si film that contains the driver circuit array that is directly bonded on bulk PLZT. The top view of a Si PLZT S-SLM and the cross section of one of its unit cells are illustrated in Fig. 1.

We investigated two direct-bonding (DB) techniques for combining thin silicon films with bulk PLZT:

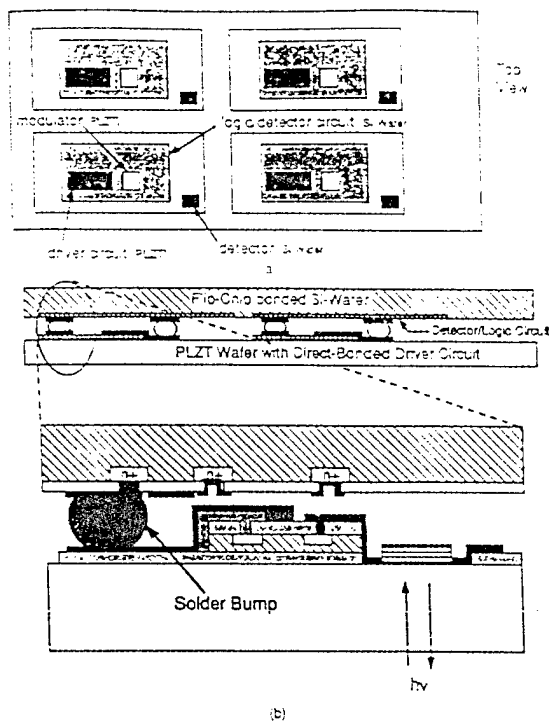DB1: Bonding of commercially available 2–4-μm-

Fig. 1. (a) Top view of a Si/PLZT S-SLM with four cells in a 2 × 2 array. (b) Cross section of one unit cell of a Si/PLZT S-SLM. A thin Si film with a driver circuit is bonded directly to bulk PLZT and flip-chip bonded to a Si wafer with detector and logic circuits.

thick Si films onto PLZT, followed by fabrication of metal-oxide-semiconductor (MOS) devices. This method utilizes thicker Si films (2–4 μm thick) that will permit the realization of more efficient Si detectors for optical addressing.

DB2: Fabrication of MOS devices in Si-on-insulator (SOI) silicon wafers, followed by lift-off of thin silicon film-containing devices and bonding to bulk PLZT. This approach permits the implementation of conventional Si device processing steps.

After the bonding was completed, modulator windows were defined through the bonding layers, and a layer of metal was deposited to make an electrical connection between the transistors and the PLZT substrate.

Lift-off of epitaxial device layers from their host semiconductor substrates followed by van der Waals bonding to other substrates has become a well-established technology for III-V compound semiconductors.[5-10] There, most of the device fabrication processes are performed before the transfer and bonding of semiconductor layers. This circumvents the stress buildup at the bonding interface that can result from high-temperature processing steps. For Si and PLZT systems, this technology had to be modified as described above for DB1 and DB2 methods in order to accommodate the change in materials involved. Both methods proved to be fruitful, and as a consequence, we were allowed to choose between the two by considering manufacturing issues such as

desired device, yield, scalability, and required processing time. Here we present the experimental outline and the outcome of both bonding methods before emphasizing a particular method, as they are both new processing technologies that may be explored for various optoelectronic applications.

2. Outline of Experiments

For the first method (DB1), we developed a processing technique to bond a Si film to a PLZT substrate and fabricate N-channel MOS (NMOS) devices through a series of low-temperature MOS processing steps that prevent thermal damage to the PLZT substrate. For this purpose, a clean 2-in.- (5.08-cm-) diameter, 4-μm-thick silicon film from Virgina Semiconductor Inc. was van der Waals-bonded to a PLZT substrate with a 20-nm-thick Al_2O_3 buffer layer (see Fig. 2) and sequenced through a low-temperature (< 850 °C), metal gate NMOS transistor fabrication process that can be found in Refs. 11 and 12. The processing temperature is lowered to satisfy the thermal restriction imposed by the PLZT. A portion of a plasma-enhanced chemical-vapor deposition-grown SiO_2 film, which serves as an ion implantation mask, provides additional support to supplement the van der Waals bonding. For comparison purposes, we have repeated the experiment with a sapphire substrate (instead of PLZT).
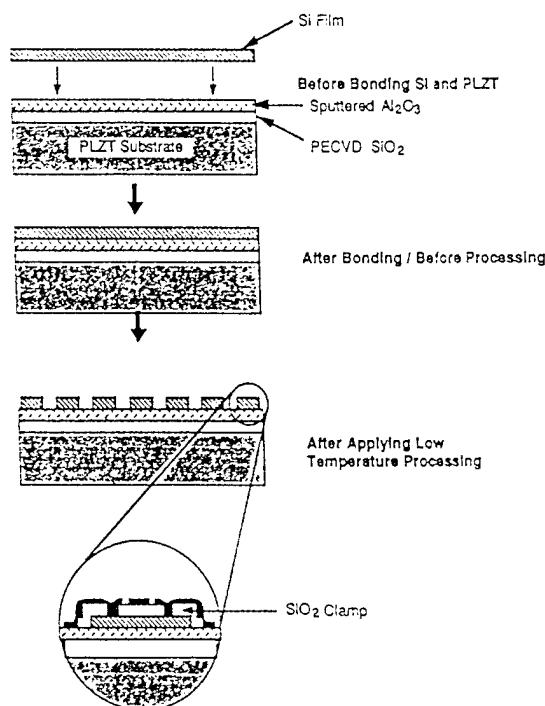

Fig. 2. Schematic illustration of processing steps involved in bonding thin Si wafers to bonded PLZT/sapphire substrates (DB1). A low-temperature processing (~850 °C compared with a typical value of 1050 °C) gate oxidation step is applied to fabricate transistor structures on the transferred Si film after bonding. PECVD, plasma-enhanced chemical vapor deposition.
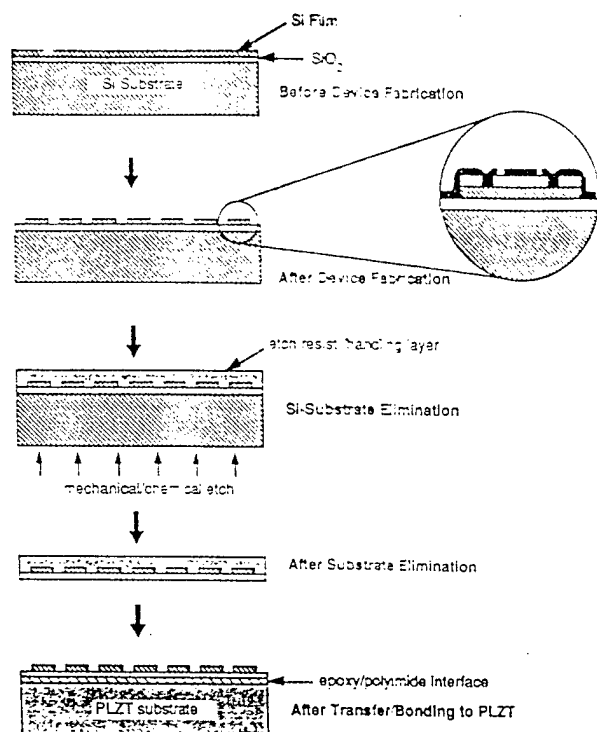
Fig. 3. Schematic illustration of processing steps involved in thinning, transferring, and bonding preprocessed Si device film onto a PLZT substrate (DB2). In this approach, any conventional Si processing step may be applied.

In the second approach (DB2), devices fabricated on the top layer (0.6–1.0-μm-thick Si) of commercially available SOI wafers are lifted off and bonded onto a PLZT substrate. The steps involved in this approach are illustrated in Fig. 3. Mechanical grinding and selective plasma etching are used to remove the host Si substrate of the SOI Si wafer. The resulting film, which consists of isolated Si islands on a SiO_2 layer, is transferred onto a PLZT substrate and is bonded with an adhesion layer of epoxy.[13] Additional metallization and photolithography are then applied to etch and contact the modulator windows. This approach permits conventional Si processing steps to be applied during device fabrication. The advantage of imposing no limitation on the MOS processing parameters is self-evident.

3. Experimental Results

Owing to the high qualities of Si films, the potential yields of both bonding methods are high. Previously, in collaboration with the Kopin Corporation,[14] we have demonstrated the possibility of transferring and bonding large device areas up to 30 × 30 mm² that contain 25 transistors mm² with near 100% yield.

Test circuits consisting of metal gate NMOS structures of various gate widths and lengths were fabricated. For comparison, reference samples were fabricated in bulk Si and in the transferred silicon-on-sapphire substrates along with the samples on PLZT

substrates. The electrical performances of NMOS structures on various substrates were compared to evaluate the potentials of direct bonding methods, and are given in Subsections 3.A and 3.B. Changes in threshold voltage V_T, drain-source breakdown voltage V_B, leakage current, and transconductance were measured for this comparison. Subsection 3.C presents the measured performance of transistors (fabricated by the use of the DB2 method) connected in a simple driver circuit configuration.

After the electrical characterization, the performance of the modulators in a fully integrated Si transistor PLZT structure was measured and compared with a reference modulator structure. The reference structure consisted of a modulator window defined and connected electrically on a polyimide layer (1 μm thick) cured on a PLZT substrate to simulate the Si/PLZT-integrated SLM structure without having the direct bonding steps applied to it. The results are given in Subsection 3.D.

A. Characteristics of N-Channel Metal-Oxide-Semiconductor Transistors Fabricated in Bonded Silicon Film (DB1)

A photomicrograph of NMOS test circuits fabricated on 4-μm-thick Si films (obtained from Virginia Semiconductors) bonded to PLZT with a 20-nm-thick sputtered Al_2O_3 layer as an interface is shown in Fig. 4. The NMOS process included a 850 °C pyrogenic oxidation step. Bonded Si-films withstood this high-temperature step, which affirms the reliability of the bonding. NMOS transistors fabricated in the bonded Si film exhibited electrical characteristics that were comparable with those of similar devices fabricated on bulk Si.[12] The threshold voltages were narrowly distributed between 1.0 and 1.2 V. The drain-source breakdown showed a sharp avalanche behavior, and the breakdown voltages of these transistors were ~ 25 V and slightly increased with the increasing gate length. The leakage current per unit gate width was 2 pA/μm following the forming gas sintering. Im-
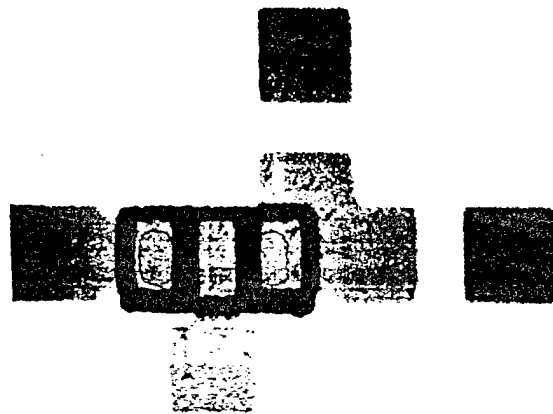

Fig. 4. Photomicrograph of an NMOS transistor fabricated on Si film bonded onto a PLZT substrate with a 20-nm-thick Al_2O_3 buffer layer (DB1).
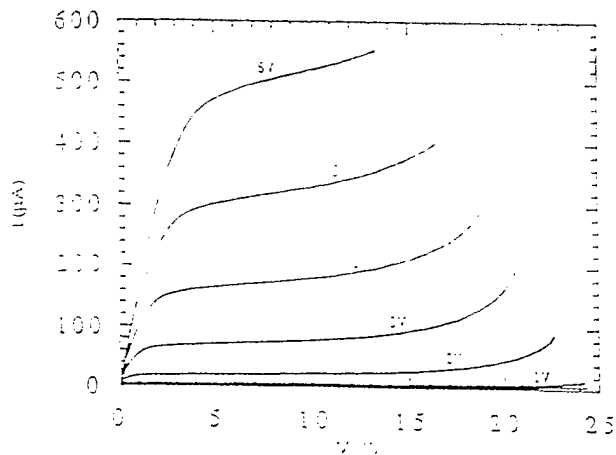
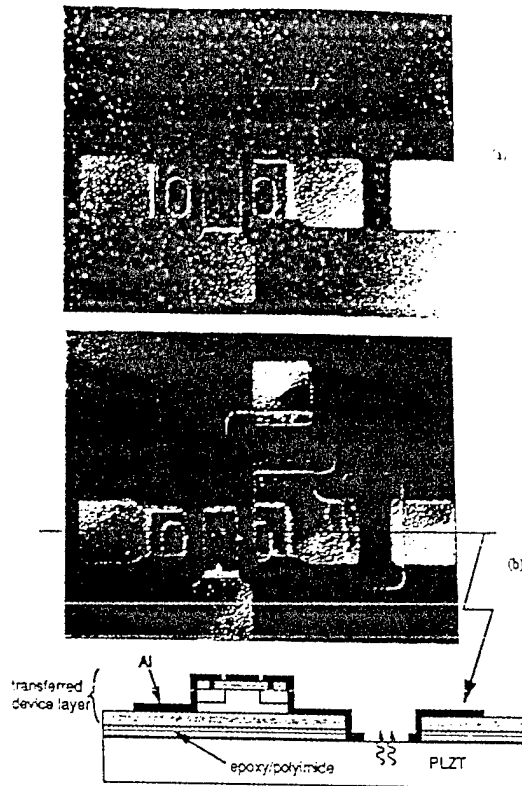Fig. 5. Typical I-V curves of a 10-μm × 20-μm gate NMOS transistor fabricated on bonded Si film (DB1).

Fig. 6. Photomicrographs of an NMOS transistor (a) on host Si-on-Si substrate before and (b) on PLZT after the etch, transfer, or bond (DB2). A cross section of the bonded structure is also illustrated.

proved processing conditions can be expected to lower the leakage current level. Figure 5 represents typical I-V curves of a 10-μm gate length and a 20-μm gate width NMOS transistor. The transconductance of these transistors was approximately 100 μS at $V_{DS} = 10$ V for $V_G = 0$–5 V (as indicated by the I-V curves in Fig. 5).

B. Characteristics of Transferred and Bonded N-Channel Metal-Oxide Semiconductor Transistors (DB2)

Utilizing the second approach (DB2), we are now able to routinely etch, transfer, and bond the 10 mm × 10 mm Si area that contains NMOS structures onto new substrates. As mentioned above, we have demonstrated the scalability of this method to device areas as large as 30 mm × 30 mm in collaboration with the Kopin Corp.[14] To minimize the step height between the PLZT modulator surface and the driving transistor that needed to be connected through a simple metal deposition step (refer to Fig. 6(b)), we used a low-viscosity (~100 cps) optical epoxy that can reduce the adhesive layer thicknesses to less than 2 μm.

Photomicrographs of MOS devices before and after etching [Figs. 6(a) and 6(b), respectively] show no discernible degradation in surface quality because of the etch, transfer, and bonding steps. The transferred devices exhibited only a slight change in electrical performance. The I-V curves of NMOS transistors of the same gate size ($W = 10$ μm and $L = 20$ μm) before and after the transfer process are compared in Fig. 7. The threshold voltage of the control sample (remaining on the SOI wafer) was in the range 0.8–0.9 V. Breakdown voltages of both control and transferred samples were ~15 V. An ~0.25-V variation in threshold voltage along with a slight increase in transconductance from 39 to 41 μS was observed at $V_{DS} = 10$ V and $V_G = 0$–5 V after the transfer. The change in the interface charge at the bonding interface is most likely the cause of the observed variations. The differences in threshold voltage and transconductance between DB1 and DB2 samples can be attributed to the difference in the doping concentrations of the substrates used for the two methods.

C. Performance of the Driver Circuit

In order to achieve variable optical modulation, we must connect the modulating medium (PLZT) and the transistors in a circuit configuration similar to that shown in Fig. 8(a). For low supply voltages (e.g., $V_{DD} = 5$ V), gate sizes for optimal gate
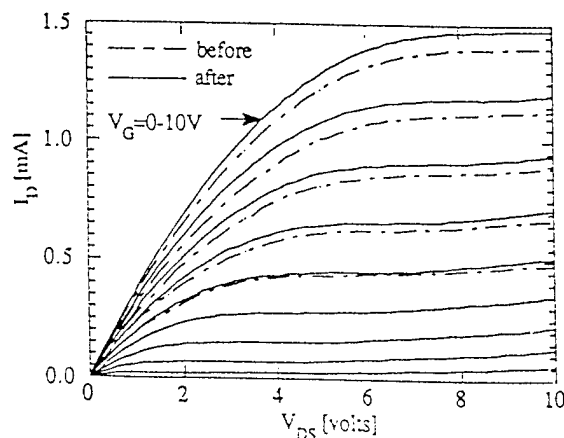

Fig. 7. I-V curves of a transistor with 10-μm-width and 20-μm-length gate size before and after the application of the etch, transfer, and bond steps (DB2).
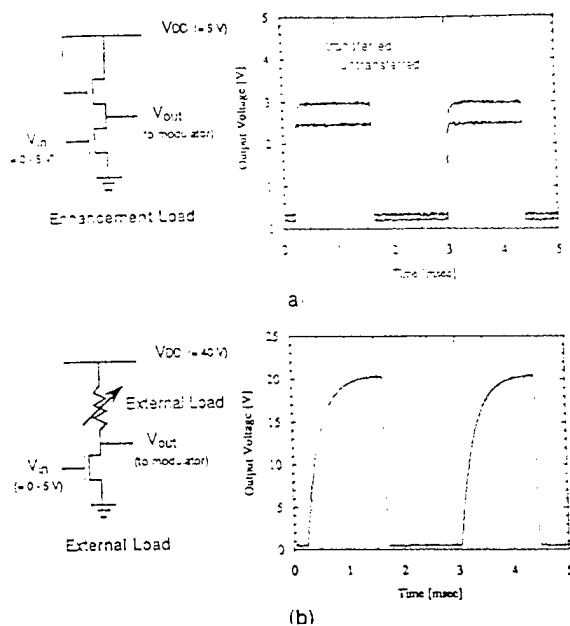
Fig. 8. Inverter connection configurations and typical output traces for 0–5-V square-wave inputs of devices processed with DB2: a Actively loaded (enhancement load) inverter. The gate sizes of the corresponding transistors were $L \times W = 20~\mu m \times 10~\mu m$ (for load transistor) and 20 $\mu m \times$ 40 μm (for inverting transistor). The output traces are that of a set of these transistors as processed on the SOI wafer (before) and after etch, transfer and bonding after). (b) Externally loaded inverter. The output trace is that of a 20 $\mu m \times$ 40 μm gate transistor after etch, transfer, and bonding.

width length ratios between the load and the inverter transistors were available on the test structure. Figure 8(a) shows the inverter configuration and the output voltage curve for a square-wave input. The curve shows a rise time of 20 μs. For supply voltages (V_{DD}) greater than 10 V, optimal gate size combinations were not available for transistor-loaded inverter connection. Thus the transistors were characterized with external load connections for measurements for which $V_{DD} > 10$ V. The measurement results given in Fig. 8(b) indicate that the maximum output swing is ~20 V for $V_{DD} = 40$ V. A further increase in V_{DD} only shifted the same swing slightly up. The breakdown voltage of transistors may be readily improved by modification of the substrate and the process parameters.

D. Performance of a Modulator that is connected to Bonded Silicon Transistor

Modulators that are 30 μm long with 15-μm electrode spacing were characterized after the final metallization step. A photomicrograph of a tested structure is shown in Fig. 6(b). Performances of this structure and a reference modulator structure are presented Figs. 9 and 10. The reference sample consisted of a 1-μm-thick polyimide that was fully cured on a PLZT (9 65 35) substrate with photolithographically defined and contacted modulators identical to those shown in Fig. 6(b). Figure 9(a) shows that at 20 and
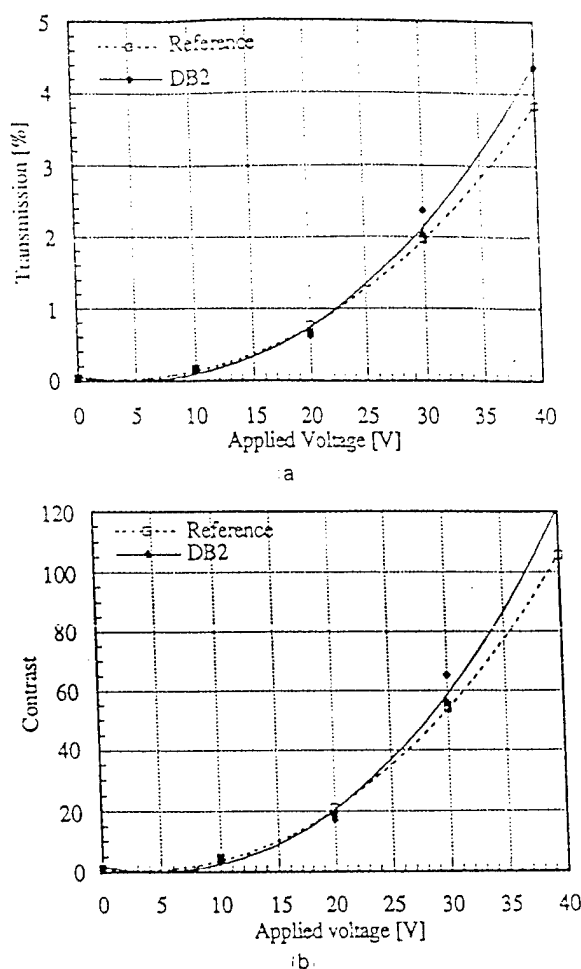

Fig. 9. Performance of modulator that is connected electrically to a transistor on Si film bonded to a PLZT substrate with DB2 compared with that of a reference modulator structure consisting of electrically connected modulator windows of the same size that are photolithographically defined on a PLZT substrate with 1-μm-thick polyimide film. (a) Optical throughput of the modulator shown in Fig. 6(b) versus applied voltage, (b) corresponding contrast ratio versus applied voltage.
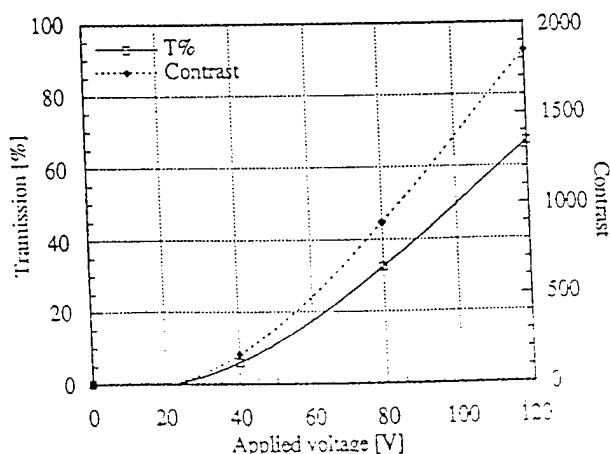

Fig. 10. Throughput and contrast of the modulator shown in Fig. 6 b as applied voltage is varied in the range 0–120 V.

40 V, transmissions rise to ~0.7% and ~4.5%, respectively, from ~0% at $V = 0$; this corresponds to contrasts of 20:1 and 120:1, respectively, as indicated by Fig. 9(b). The results correspond to previously obtained measurement values for modulators of the same size with metal contacts defined directly on PLZT.[3] When the applied voltage is increased to 120 V, the throughput is increased to ~87% with a corresponding contrast of 1800:1, as shown in Fig. 10. To achieve optimum speed and modulation depth ($\Delta T\%$ for a given ΔV), the modulator may be biased.[15] The abovementioned bonding and NMOS processing steps are demonstrated so as not to degrade the modulator performance as they were all carefully selected and modified to avoid damage to the PLZT substrate.

4. Discussion

A. Selection of Fabrication Method

Both DB1 and DB2 employ near-bulk-quality Si films. Hence logic circuits of any complexity and transistor count can be implemented into the thin Si layer. Method DB1 utilizes thicker (~4-μm) Si films that would readily accommodate the realization of an efficient detector on the film, as mentioned above. However, as all device processing steps are performed after the bonding, this method imposes a rigorous demand on the strength and the quality of the initial Si/PLZT bond. Method DB2 virtually removes this requirement as only two simple lithographic steps (modulator definition and electrical contacting) need to be applied to the structure following the bonding step. As yet, Si layer thicknesses of commercially available SOI wafers ($\leq 1 \mu$m) are not sufficient for fabrication of efficient detectors, but DB2 offers the possibility of employing conventional Si technologies for the implementation of circuits of any complexity onto the bonded device layer. Integration of a larger Si area and a PLZT substrate is possible with either method without adding complications to the processing steps.

B. Driver Circuit Simulations

In order to utilize a large array of integrated modulator and driver circuits, as in an S-SLM, each cell in the array should be individually addressable with 5-V signals from a supporting signal processing circuit. However, even the quadratic PLZT modulator requires much larger voltage swings (≥ 10 V for producing useful light modulation at a typical electrode spacing of 15 μm. Thus a large driver circuit output (> 10 V) must be variable with 0–5-V control signal. A modified inverter circuit illustrated in Fig. 11 meets these requirements as a driver circuit. This design was optimized through SPICE numerical circuit simulations. The transient characteristics of this driver are presented in Figs. 12. Figure 12(a) shows a rise time of 100 ns (or a 10-MHz response) for 1-pF modulator load capacitance. Figure 12(b) gives the driver output voltage as the gate voltage on the inverting transistor is varied in the range 0–5 V,
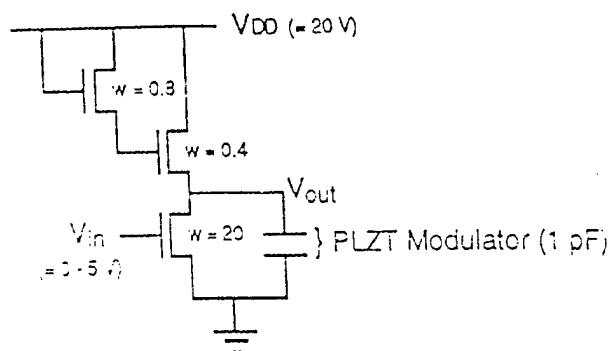

Fig. 11. Schematic illustration of a high-voltage (20-V) inverting circuit for driving PLZT modulators. w (which is width/length) represents the normalized gate widths of NMOS transistors.

demonstrating that the driver output may be used for analog operation.

C. Additional Considerations for Smart Spatial Light Modulator Fabrication

The fabrication of large-array S-SLM's demands other requirements. The addition of demultiplexer, memory cells, and XOR gates required for individually addressasble, large-array ($\geq 32 \times 32$) S-SLM's has
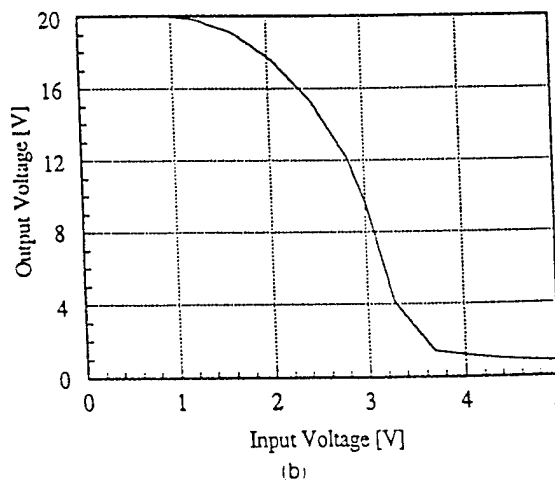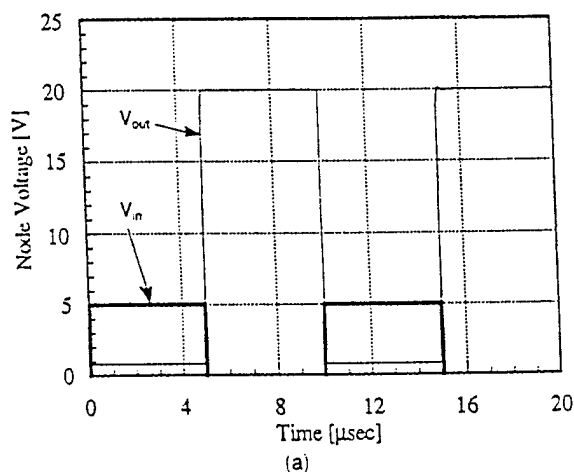

Fig. 12. SPICE simulation for the modulator driver circuit detailed in Fig. 8: (a) transient characteristics for 0–5-V square-wave input, (b) output voltage as a function of 0–5-V input variation.

been considered extensively in the past.[5] Fabrication methods presented here can readily accommodate these circuit additions. Currently we have completed the design for prototype 8 × 8 S-SLM's consisting of the discussed driver circuit and 15-μm-aperture PLZT modulators as a step toward producing sophisticated S-SLM's in the near future. After the functionality of an 8 × 8 S-SLM is demonstrated, further improvement in modulator performance will be desired. The modulator may be dc biased to maximize the modulation of depth without complicating the driver design.[15] The speed of the modulator may be increased by the implementation of a larger driver with more current handling capability.

Conclusion

The successful integration of MOS devices and PLZT substrates for self-contained SLM (consisting of Si driver circuits bonded and connected to PLZT modulators) fabrication by the use of two processing methods was demonstrated. The resulting structures exhibited electrical and optical properties comparable with those of modulator and Si devices fabricated independently in corresponding bulk substrates. The expected performance of a high-voltage (> 20-V) driver circuit was also presented. Continued study is under way to combine these technologies to produce high-speed (> 10 MHz) S-SLM's with negligible optical absorption for optical computing applications. To add complex processing capability along with better detectors to each S-SLM cell, as shown in Fig. 1, we have also been studying flip-chip bonding with improved alignment accuracy. The results of this research will be presented in a separate paper in the near future. Our objectives are to build both electrically and optically addressable S-SLM's with a direct-bonded driver and addressing circuit and a flip-chip bonded processing circuit. The achievements reported in this paperwork laid the groundwork for a unique type of S-SLM that may offer a new way of overcoming some of the limitations imposed by other optical interconnection technologies for massively parallel optical computing.

References

1. G. Moddel, K. M. Johnson, W. Li, R. A. Rice, L. A. Pagano-Stauffer, and M. A. Handschy, "High-speed binary optically addressed spatial light modulator," Appl. Phys. Lett. 55, 537–539 (1989).

2. L. K. Cotter, T. J. Drabik, R. J. Dillon, and M. A. Handschy, "Ferroelectric-liquid-crystal/silicon-integrated-circuit spatial light modulator," Opt. Lett. 15, 291–293 (1990).

3. D. Armitage and D. K. Kinell, "Liquid-crystal integrated silicon spatial light modulator," Appl. Opt. 31, 3945–3949 (1992).

4. D. Miller, L. Chirovsky, T. K. Woodward, T. Lentine, R. McCormick, and S. Hinton, "SEED principles 1 and 2," ARPA AT&T FET-SEED Workshop Notes AT&T, Newark, N.J., 1993.

5. A. Ersen, S. Krishnakumar, V. Ozguz, J. Wang, S. Esener, and S. H. Lee, "Design issues and development of monolithic silicon/lead lanthanum zirconate titanate integration technologies for smart spatial light modulators," Appl. Opt. 31, 3950–3965 (1992).

6. S. Krishnakumar, V. H. Ozguz, C. Fan, C. Cozzolino, S. C. Esener, and S. H. Lee, "Deposition and characterization of thin ferroelectric lead lanthanum zirconate titanate (PLZT) films on sapphire for spatial light modulator applications," IEEE Trans. Ultrason. Ferroelectr. Frequency Control 38, 585–590 (1991).

7. W. Van der Wel, R. Buchner, K. Habenerger, S. Seitz, J. Weber, and P. Seegebrecht, "Avoidance of substrate damage upon laser recrystallization of a SOI layer," J. Electrochem. Soc. 138, 1117–1122 (1991).

8. E. Yablonovitch, D. M. Wang, T. J. Gmitter, and L. T. Florez, "Van der Waals bonding of GaAs epitaxial lift-off films on to arbitrary substrates," Appl. Phys. Lett. 56, 2419 (1990).

9. A. Yi-Yan, W. K. Chan, T. J. Gmitter, L. T. Florez, J. L. Jackel, E. Yablonovitch, R. Bhat, and J. P. Harbison, "Grafted GaAs detectors on lithium niobate and glass optical waveguides," IEEE Photon. Tech. Lett. 1, 379–380 (1989).

10. C. Camperi-Ginestet, M. Hargis, N. Jokerst, and M. Allen, "Alignable epitaxial liftoff of GaAs material with selective deposition using polyimide diaphragms," IEEE Photon. Tech. Lett. 3, 1123–1126 (1991).

11. G. P. Imthurn and G. A. Garcia, "Bonded silicon-on-sapphire wafers and devices," J. Appl. Phys. 72, 2526–2527 (1992).

12. J. H. Wang, M. S. Jin, V. Ozguz, and S. H. Lee, "N-channel metal-oxide-semiconductor transistors fabricated in a silicon film bonded onto sapphire," Appl. Phys. Lett. (to be published).

13. Y. Hayashi, S. Wada, K. Kajiyana, K. Oyama, R. Koh, S. Takahashi, and T. Kunio, "Fabrication of three-dimensional IC using cumulatively bonded IC (CUBIC) technology," in Proceedings of the 1990 Symposium on VLSI Technology (Institute of Electrical and Electronics Engineers, New York, 1990), pp. 95–96.

14. M. S. Jin, J. H. Wang, V. H. Ozguz, and S. H. Lee, "Bonding of Si thin films to PLZT substrates for smart spatial light modulator applications," in Spatial Light Modulators and Applications, Vol. 6 of 1993 OSA Technical Digest Series (Optical Society of America, Washington, D.C., 1993), pp. 123–126.

15. B. Mansoorian, G. Marsden, V. Ozguz, C. Fan, and S. Esener, "Characterization of a free-space optoelectronic interconnect system based on Si PLZT smart pixels," in Spatial Light Modulators and Applications, Vol. 6 of 1993 OSA Technical Digest Series (Optical Society of America, Washington, D.C., 1993), pp. 128–131.